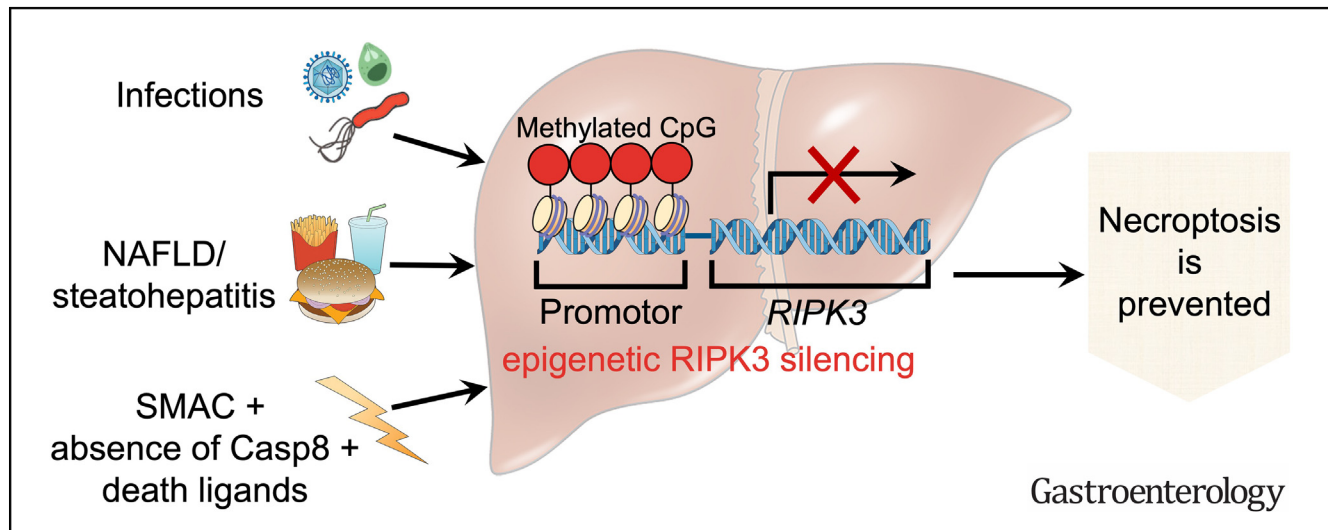




Epigenetic Silencing of RIPK3 in Hepatocytes Prevents MLKL-mediated Necroptosis From Contributing to Liver Pathologies

Simon P. Preston,^{1,2} Michael D. Stutz,^{1,2} Cody C. Allison,^{1,2} Ueli Nachbur,^{1,2} Quentin Gouil,^{1,2} Bang Manh Tran,³ Valerie Duvivier,⁴ Philip Arandjelovic,^{1,2} James P. Cooney,^{1,2} Liana Mackiewicz,¹ Yanxiang Meng,^{1,2} Jan Schaefer,^{1,2} Stefanie M. Bader,^{1,2} Hongke Peng,^{1,2} Zina Valaydon,^{1,2} Pravin Rajasekaran,^{1,2} Charlie Jennison,^{1,2} Sash Lopaticki,¹ Ann Farrell,⁵ Marno Ryan,⁵ Jess Howell,⁵ Catherine Croagh,⁵ Denuja Karunakaran,^{6,7} Carole Schuster-Klein,⁴ James M. Murphy,^{1,2} Theodora Fifis,⁵ Christopher Christophi,⁵ Elizabeth Vincan,^{3,8,9} Marnie E. Blewitt,^{1,2} Alexander Thompson,⁵ Justin A. Boddey,^{1,2} Marcel Doerflinger,^{1,2,§} and Marc Pellegrini^{1,2,§}

¹Walter and Eliza Hall Institute of Medical Research, Parkville, Victoria, Australia; ²Department of Medical Biology, The University of Melbourne, Parkville, Victoria, Australia; ³Department of Infectious Diseases, The University of Melbourne, The Peter Doherty Institute for Infection and Immunity, Melbourne, Victoria, Australia; ⁴Cardiovascular and Metabolic Disease Center for Therapeutic Innovation, SERVIER Group, Suresnes, France; ⁵Department of Gastroenterology, St. Vincent's Hospital, The University of Melbourne, Melbourne, Victoria, Australia; ⁶Institute for Molecular Bioscience, University of Queensland, St Lucia, Queensland, Australia; ⁷Monash Biomedicine Discovery Institute and Victorian Heart Institute, Monash University, Clayton, Victoria, Australia; ⁸Victorian Infectious Disease Reference Laboratory, The Peter Doherty Institute for Infection and Immunity, Melbourne, Victoria, Australia; and ⁹Curtin Medical School, Curtin University, Perth, Western Australia, Australia



See editorial on page 1492.

BACKGROUND & AIMS: Necroptosis is a highly inflammatory mode of cell death that has been implicated in causing hepatic injury including steatohepatitis/ nonalcoholic steatohepatitis (NASH); however, the evidence supporting these claims has been controversial. A comprehensive, fundamental understanding of cell death pathways involved in liver disease critically underpins rational strategies for therapeutic intervention. We sought to define the role and relevance of necroptosis in liver pathology. **METHODS:** Several animal models of human liver pathology, including diet-induced steatohepatitis in male mice and diverse infections in both male and female mice, were used to dissect the relevance of necroptosis in liver pathobiology. We applied

necroptotic stimuli to primary mouse and human hepatocytes to measure their susceptibility to necroptosis. Paired liver biospecimens from patients with NASH, before and after intervention, were analyzed. DNA methylation sequencing was also performed to investigate the epigenetic regulation of RIPK3 expression in primary human and mouse hepatocytes. **RESULTS:** Identical infection kinetics and pathologic outcomes were observed in mice deficient in an essential necroptotic effector protein, MLKL, compared with control animals. Mice lacking MLKL were indistinguishable from wild-type mice when fed a high-fat diet to induce NASH. Under all conditions tested, we were unable to induce necroptosis in hepatocytes. We confirmed that a critical activator of necroptosis, RIPK3, was epigenetically silenced in mouse and human primary hepatocytes and rendered them unable to undergo necroptosis.

CONCLUSIONS: We have provided compelling evidence that necroptosis is disabled in hepatocytes during homeostasis and in the pathologic conditions tested in this study.

Keywords: Necroptosis; Cell Death; NASH; Chronic Infection; RIPK3.

Two of the main driving biological processes that underpin liver disease are persistent inflammation and aberrant cell death.^{1,2} The death of hepatocytes during chronic and acute liver disease can involve apoptosis and necrosis. Over the past 18 years, a programmed form of necrosis has been described called necroptosis. This lytic form of cell death has controversially been implicated in both acute and chronic liver disease.^{1–3} Necroptosis has been strongly implicated in nonalcoholic fatty liver disease (NAFLD) and nonalcoholic steatohepatitis (NASH) in both animal models and human disease for almost a decade.^{2,4} NAFLD is the most common disease in the Western world, affecting up to 40% of the general population that in many cases develops into NASH and/or hepatocellular carcinoma.⁵

Necroptotic death can be induced downstream of death receptor signaling. Toll-like receptor activation and some viral pathogens can induce necroptosis through multiple mechanisms.^{6–8} The essential initiator and effector of necroptosis are the proteins, receptor interacting protein kinase 3 (RIPK3), and mixed lineage kinase domain-like pseudokinase (MLKL), respectively.^{9–11} Death ligands, such as tumor necrosis factor (TNF) superfamily members, engage their cognate receptors to initiate one of several mutually exclusive events, including activation of nuclear factor- κ B, induction of apoptosis, and induction of necroptosis.¹² Necroptosis will only occur downstream of death receptor ligation if there is loss of caspase-8 function and, generally, a concurrent loss of cellular inhibitor of apoptosis (cIAP) protein function.^{9,13} Normally, caspase-8 and cIAPs prevent the accumulation of activated RIPK3. Once activated, RIPK3 phosphorylates MLKL, which then disrupts cell membrane integrity to cause necroptotic death.^{9,14–17}

MLKL is expressed in almost all cell types, and protein expression is regulated by type I and II interferon signaling.^{18–20} Although underexplored, MLKL has been proposed to serve roles beyond necroptosis, including a potential role in restricting replication of intracellular pathogens.²¹ Unlike MLKL, RIPK3 is not ubiquitously expressed but is most highly expressed in the hematopoietic system, skin, and gastrointestinal tract.²² RIPK3 protein and transcripts are not detectable in some primary tumors and several cancer cell lines. This has been attributed to hyper-methylation of the promoter region of *RIPK3* and is associated with transcriptional repression.^{23,24} It is not known if similar mechanisms are responsible for regulating RIPK3 expression in noncancerous tissues.

The momentum in developing inhibitors of necroptosis for the potential treatment of liver disease has been growing, but a lack of fundamental insights limits our knowledge of their potential clinical applicability. Indeed, robust RIPK3 expression is essential for necroptosis, yet several publications indicate that hepatocytes do not

WHAT YOU NEED TO KNOW

BACKGROUND AND CONTEXT

The role for necroptosis in causing liver pathology has been controversial, and we attempt to clarify the relevance of this form of cell death.

NEW FINDINGS

We show that epigenetic silencing of RIPK3 restricts necroptosis in mouse and human hepatocytes across multiple hepatic pathologies, including infection and steatohepatitis.

LIMITATIONS

Human liver organoids are not a good model to study necroptotic cell death in liver pathologies.

CLINICAL RESEARCH RELEVANCE

We provide compelling evidence that informs rational strategies for therapeutic intervention targeting necroptosis in liver diseases.

BASIC RESEARCH RELEVANCE

Our findings that epigenetic silencing of RIPK3 restricts necroptosis in hepatocytes may guide interpretation of results of basic research into a range of liver pathologies.

express RIPK3 protein.^{25,26} Intriguingly, liver conditional caspase-8 gene targeting and pharmacological inhibition of caspase function, both potential triggers for necroptosis, do not cause any liver abnormalities in animals. To the contrary, these animals are refractory to TNF- and FASL-driven fatal hepatitis.^{17,27,28} However, it is possible that inflammation associated with pathogenesis of disease could alter the conditions such that necroptosis is favored. This study aims to definitively determine the role of necroptosis across several important liver pathologies.

Materials and Methods

Ethics Approvals

The Walter and Eliza Hall Institute Animal Ethics Committee reviewed and approved all animal experiments conducted

[§] These authors share co-last authorship.

Abbreviations and Acronyms: ALT, alanine transaminase; AST, aspartate transaminase; BMDM, bone marrow derived macrophages; CC3, cleaved caspase 3; CDAHFD, choline deficient L-amino acid defined high fat diet; cIAP, cellular inhibitor of apoptosis; HBV, hepatitis B virus; H&E, hematoxylin-eosin; HFD, high-fat diet; HuLiver, human liver chimeric mouse; LCMV, lymphocytic choriomeningitis virus; MLKL, mixed lineage kinase domain-like pseudokinase; mRNA, messenger RNA; NAFLD, non-alcoholic fatty liver disease; NASH, nonalcoholic steatohepatitis; PHH, primary human hepatocyte; RIPK3, receptor interacting serine/threonine protein kinase 3; SMAC, second mitochondria derived activator of caspases; TNF, tumor necrosis factor; TUNEL, terminal deoxynucleotidyl transferase dUTP nick end labeling; WT, wild type.

Most current article

© 2022 The Author(s). Published by Elsevier Inc. on behalf of the AGA Institute. This is an open access article under the CC BY-NC-ND license (<http://creativecommons.org/licenses/by-nc-nd/4.0/>).

0016-5085

<https://doi.org/10.1053/j.gastro.2022.08.040>

at the institute. The University of Queensland Animal Ethics Committee approved all experiments performed at the Institute for Molecular Biosciences at The University of Queensland. The Walter and Eliza Hall Institute Human Research and Ethics Committee reviewed and approved all work involving primary human liver cells performed at the institute. Human liver tissues were provided by the Department of Surgery at the Austin hospital with the approval of the Austin hospital human research ethics committee and from the Department of Gastroenterology at St. Vincent's hospital with the approval of the St. Vincent's hospital human research ethics committee.

Animal Infections

Mice used in experiments were aged between 6 and 12 weeks. The sex of animals is indicated in the text below and legends accompanying the relevant figures. Gene-targeted animals used in our experiments were all on a C57BL/6J (H-2D^b) background and have been described elsewhere.^{17,27,28} Humanized liver (HuLiver) mice were obtained from Yecuris Corporation (Tulatin, OR). HuLiver mice were female C57BL/6J FRG (*Fah*^{-/-} *Rag2*^{-/-} *IL2Rγ*^{-/-}) repopulated with primary human hepatocytes (PHHs). HuLiver mice or C57BL/6J mice were infected with 2×10^6 plaque-forming units of lymphocytic choriomeningitis virus (LCMV) Docile by intravenous injection into the tail vein. LCMV Docile was propagated on L929 cells. Mouse hepatitis B virus (HBV) infection was induced by hydrodynamically injecting 10 µg of plasmid encoding HBV genotype A (pAAV-HBV1.2) in a volume of phosphate-buffered saline equivalent to 8% of the mouse body weight into the tail vein of male and female mice.²⁹ *Plasmodium berghei* infections were performed by dissecting sporozoites from the salivary glands of *Anopheles stephensi* mosquitos 19 to 22 days post infection. Sporozoites were resuspended in RPMI 1640 (ThermoFisher Scientific, Waltham, MA) and 3000 sporozoites were intravenously injected into the tail vein of male and female Swiss Webster mice. This method has been described elsewhere.³⁰

Results

MLKL Expression Is Enhanced During Infection With Hepatotropic Pathogens

Infections promote type I interferon production, which can prime necroptosis in certain settings.^{18,31} Mice infected with hepatotropic LCMV and HBV show upregulation of liver MLKL protein expression compared with uninfected mice (Figure 1A) and compared with mice with a highly constrained *P. berghei* sporozoite infection. The inability to detect perturbations in MLKL levels in whole liver lysates from *P. berghei* infected mice may just reflect the very low number of hepatocytes that are infected in this model. Our data suggest that some infections can prime hepatic necroptosis by modulating MLKL protein levels. Necroptosis has been implicated in causing disease across several liver infections, so we next sought to confirm this by using gene-targeted animals that are deficient in MLKL.^{2,32}

MLKL^{-/-} Livers Develop Normally and Necroptosis Does Not Affect the Pathogenesis of HBV Infection

MLKL^{-/-} mice have identical liver histological architecture and cellular composition compared with wild-type

(WT) mice (Supplementary Figure 1A-E). We induced persistent HBV infection in animals as previously described^{29,33} and noted similar levels of infection across mouse genotypes (Figure 1B and Supplementary Figure 1F). Plasma transaminase levels were used as surrogate markers for hepatocyte dysfunction and death, and we observed equivalent levels of aspartate transaminase (AST) in WT and *MLKL*^{-/-} animals (Figure 1C). These data indicated that necroptosis was not contributing to hepatocyte dysfunction/death during HBV infection. MLKL deficiency did not perturb immune-mediated inflammatory responses to HBV infection (Figure 1D and E). WT and MLKL deficient mice made comparable levels of serum anti-HBV surface antigen (anti-HBs) antibodies (Supplementary Figure 1G) and controlled infection with similar kinetics (Figure 1F). Cleaved caspase-3 (CC3) staining was used to detect apoptosis in infected livers and the loss of MLKL did not affect this form of cell death (Figure 1G). These data indicate that necroptosis plays no physiological role in HBV infection and disease based on our model.

Necroptosis Does Not Contribute to Liver Pathology Associated With LCMV Infection

High-titer LCMV Docile infection in mice causes persistent inflammation in the liver. LCMV is noncytopathic, so any end-organ damage is the consequence of innate and adaptive immune responses targeting infected cells. Similar to HBV infection, MLKL loss did not affect liver immune cell infiltration and LCMV-specific glycoprotein and nucleoprotein adaptive immune responses (Figure 2A-C). The activation phenotype of T cell responses (CD69 and PD-1 expression) was comparable across infected *MLKL*^{-/-} and WT mice (Figure 2D).

To assess the extent of inflammation-driven liver pathology, hepatocyte death, and specifically apoptosis, we performed hematoxylin-eosin (H&E) staining, terminal deoxynucleotidyl transferase dUTP nick end labeling (TUNEL), and CC3 staining (Figure 2E). We also measured serum AST, inflammatory cytokine levels, and viral titers. The results of all assays were equivalent across infected WT and *MLKL*^{-/-} mice (Figure 2F-H and Supplementary Figure 2A and B). Collectively, these data indicated that necroptosis plays no physiologically relevant role in the pathogenesis of LCMV liver disease. We extended our analysis beyond the liver and assessed immune responses and viral loads in the spleen and found no differences between MLKL-deficient mice and WT animals (Supplementary Figure 2F).

Necroptosis Does Not Affect Liver-Stage Infection by Malaria Parasites

Although sporozoite infection did not perturb MLKL protein levels in whole liver lysates, we nonetheless sought to understand if necroptosis could contribute to the hepatic life cycle and pathology caused by malaria.³⁴ We did not observe any differences in liver parasite burdens and no differences in serum AST levels when we compared *P. berghei*-infected WT and *MLKL*^{-/-} mice (Supplementary Figure 3A and B). Progression to blood stage and illness

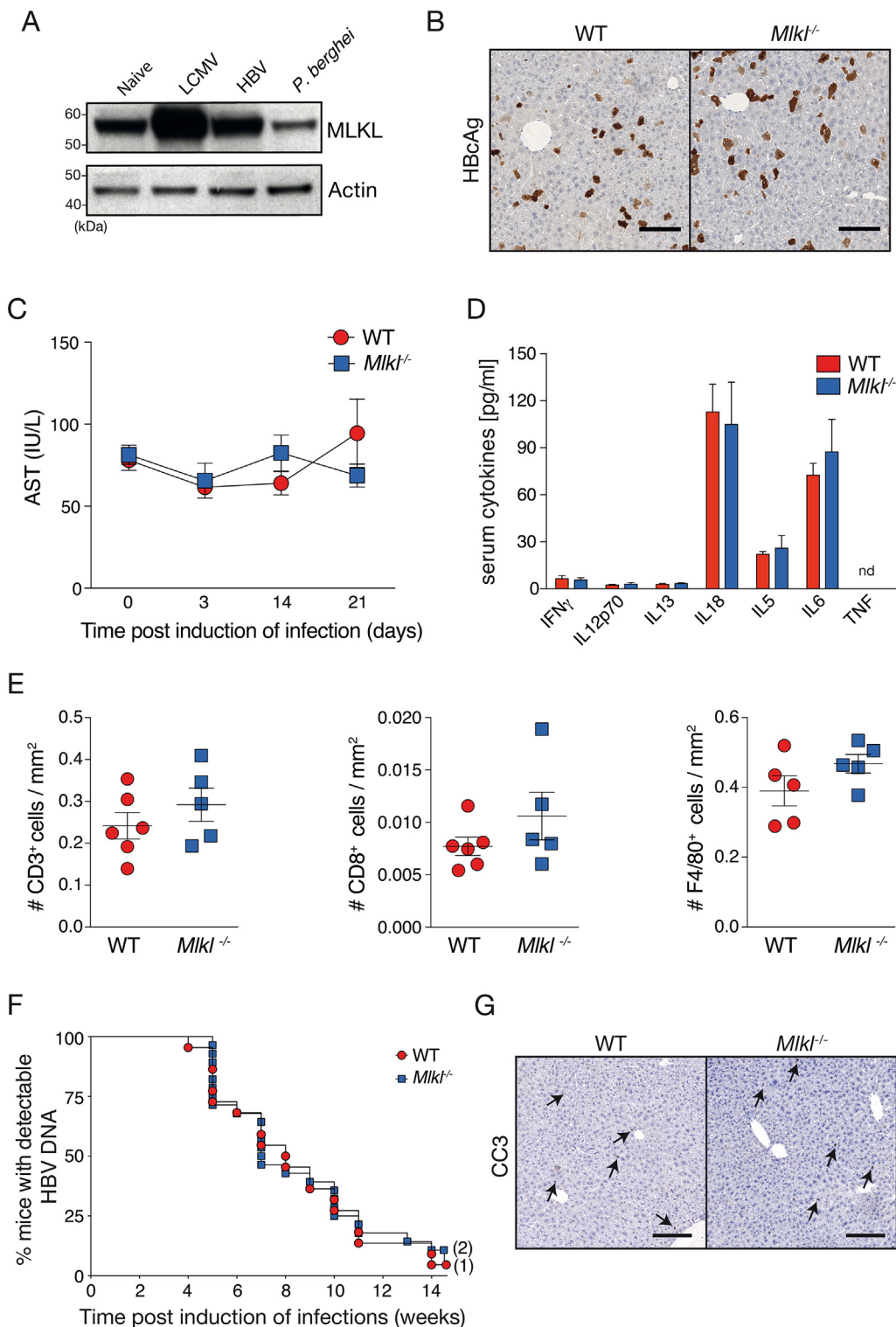


Figure 1. Liver MLKL expression is enhanced following infection with some pathogens but clearance of chronic HBV occurs independently of necroptosis in mice. (A) Western blot of MLKL total protein expression in whole liver lysates from naïve mice or postinfection with LCMV Docile (8 days), HBV (14 days), or *P. berghei* (44 hours). (B) Representative images of liver sections stained for HBV core antigen (HBcAg) by immunohistochemistry. (C) Serum AST levels from naïve or HBV-infected mice at the indicated time points ($n = 4\text{--}10$ mice per time point). (D) Concentrations of the indicated serum cytokines from HBV-infected mice ($n = 5\text{--}10$). (E) Total number of T cells (CD3 $^{+}$), cytotoxic T cells (CD8 $^{+}$), or Kupffer cells (F4/80 $^{+}$) in liver sections as determined by immunohistochemistry. (F) Proportion of animals and time when mice first achieved an undetectable serum HBV DNA level ($n = 22\text{--}28$). Numbers next to dots in the time to event analyses represent remaining mice that have not cleared HBV. (G) Representative liver sections stained for CC3 by immunohistochemistry. Arrows indicate apoptotic cells. Data in (B, D, E, G) were obtained from mice of mixed gender, 14 days postinfection with HBV. Graphs show mean and SEM. Scale bar in (B) and (G): 125 μm .

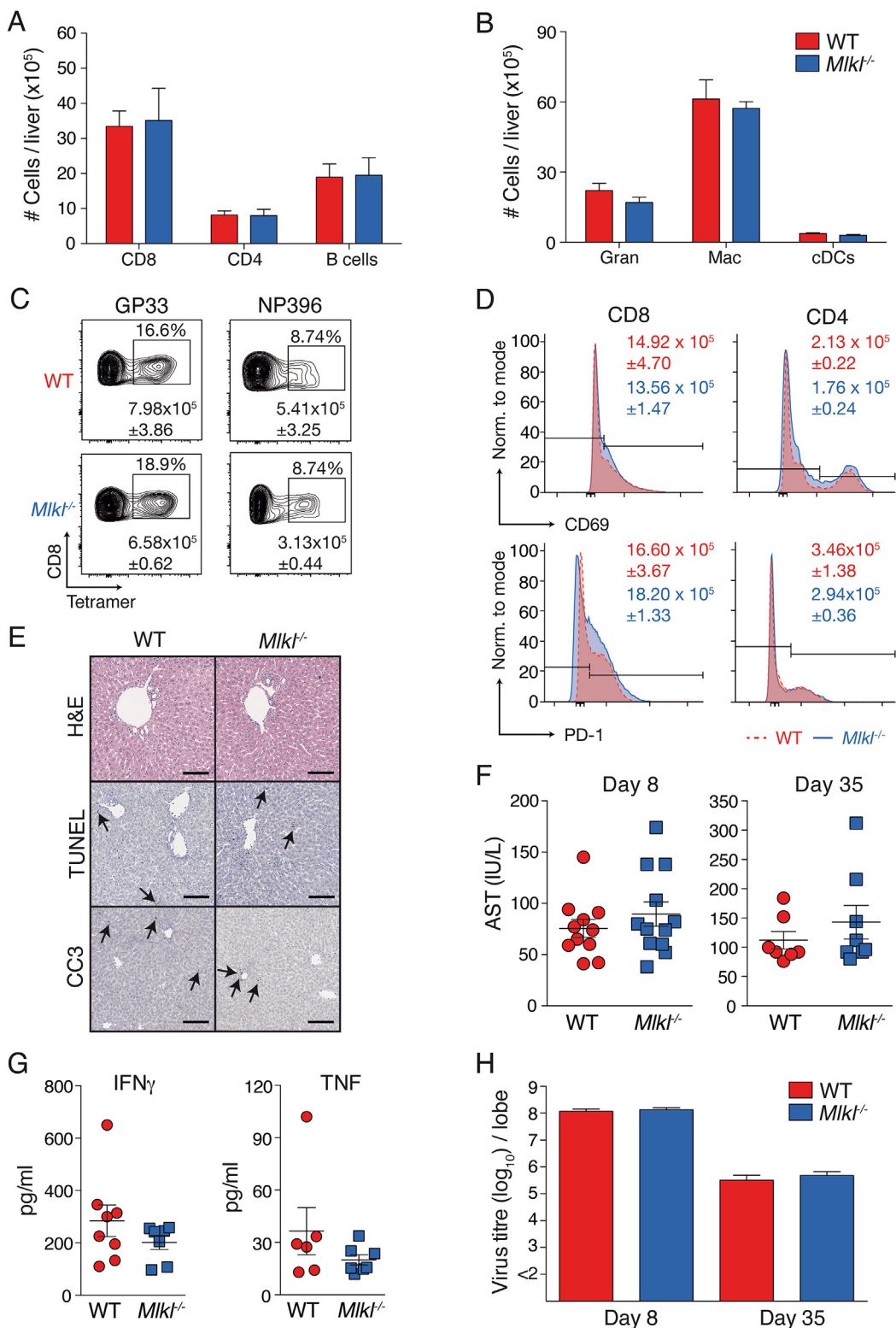
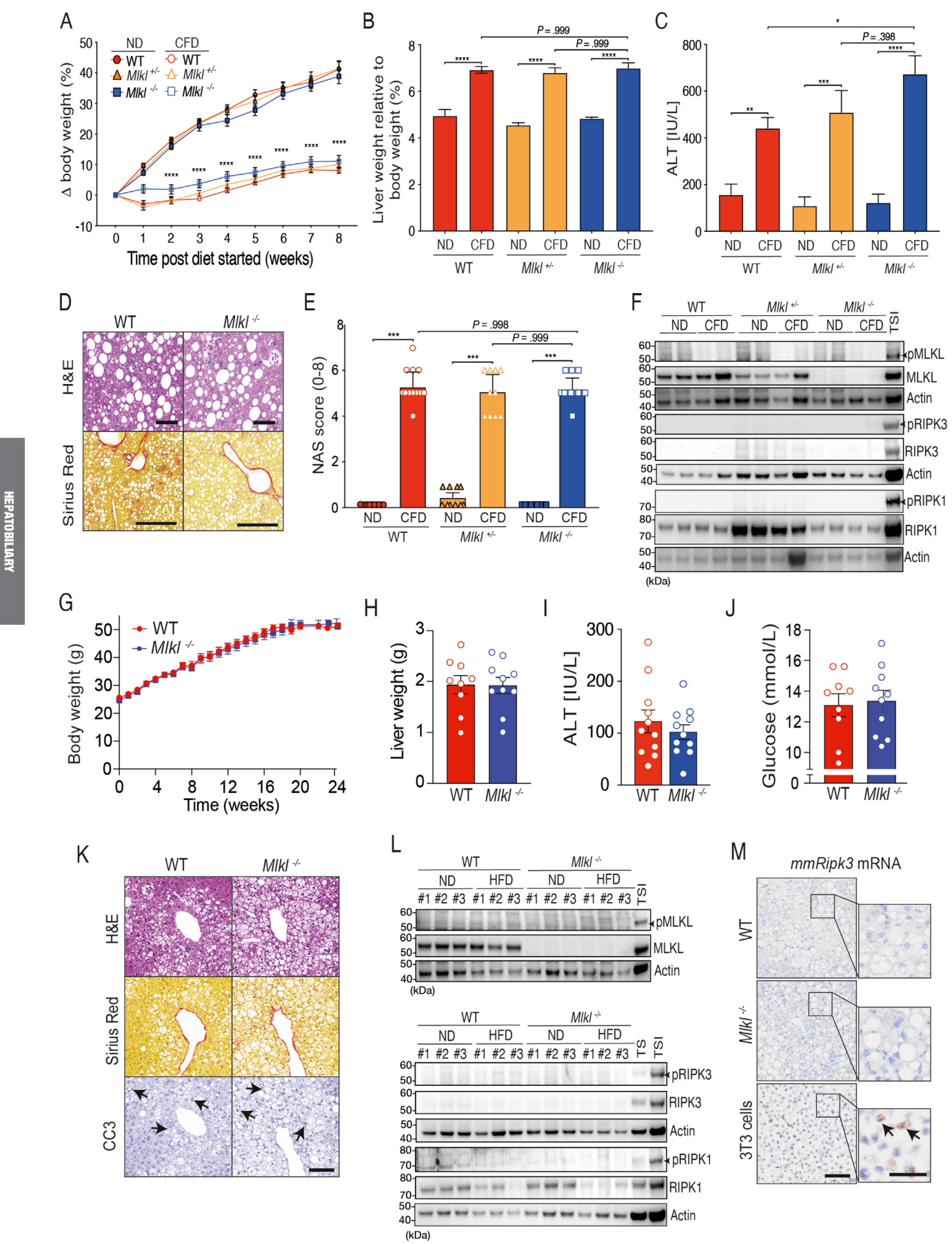


Figure 2. MLKL deficiency does not alter immunity to LCMV in the liver. (A and B) Flow cytometric determination of the absolute number of immune cells. (C) Proportion and absolute number of LCMV-specific CD8 $^{+}$ T cells ($n = 4$). (D) Proportion and absolute number of T cells that express CD69 or PD-1 ($n = 4$). (E) Histological liver sections stained with H&E or with antibodies recognizing total cell death (TUNEL) or apoptosis (CC3). Arrows indicate dead/dying cells ($n = 8$ mice per group). Scale bar: 125 μ m. (F) Serum levels of AST from mice at days 8 and 35 postinfection. (G) Serum cytokine levels in LCMV-infected mice. (H) Virus titers at days 8 and 35 postinfection ($n = 8$). All data were generated from livers of mice of mixed gender, taken 8 days postinfection with LCMV Docile, unless otherwise specified. Flow cytometry plots (C and D) and images (E) are representative of 8 analyses performed on independent mice. Data are representative of 2 independent experiments (A–E) or the combined data of 2 independent experiments (F–H). Graphs showing summary data indicate the mean and SEM. cDC, conventional dendritic cell (CD11c $^{+}$ MHC-II $^{+}$); Gran, granulocyte (CD11b $^{+}$ Gr-1 HI); IFN, interferon; Mac, inflammatory macrophage (CD11b $^{+}$ Gr-1 INT).



occurred at the same time in infected WT and *Mlk1*^{-/-} animals (Supplementary Figure 3C). Collectively, our data showed that the absence of necroptosis did not affect any of the processes required for sporozoite transmission and progression to blood stage.

Necroptosis Does Not Contribute to NAFLD or NASH Pathology in Mouse Models

Necroptosis has been repeatedly hypothesized to contribute to the development of NAFLD and progression to NASH, cirrhosis, and long-term sequelae, such as hepatocellular carcinoma.^{1,2,4,35} However, many of these studies used drugs or mice with genetic deficiencies that are likely to have off-target or additional and poorly understood consequences. Furthermore, other factors such as the microbiome and sex-related hormones have been postulated to affect results in these models.^{36,37} Therefore, we sought to directly determine if necroptosis contributed to the liver pathology and progression to steatohepatitis using well-established mouse models of NASH.

We fed animals a well-accepted choline-deficient, L-amino-acid defined, high-fat diet (CDAHFD) or high-fat diet (HFD, 60% kcal) containing standard levels of choline and amino acids and a normal diet. For all experiments with CDAHFD, we intercrossed *Mlk1*^{+/+} mice to generate *Mlk1*^{-/-} mice and MLKL-sufficient littermate controls to ensure a consistent genetic and environmental background. Compared with animals fed a normal diet, mice fed CDAHFD for 8 weeks struggled to gain weight and had visibly pale, fatty livers (Figure 3A and Supplementary Figure 4A and B). There were no differences between MLKL-deficient or -sufficient mice fed CDAHFD across all experimental measures of steatohepatitis-related illness, including liver-to-body weight ratio, total liver weights, liver damage as determined by the levels of plasma AST and alanine transaminase (ALT), and important metabolic parameters in the blood and livers of mice (alkaline phosphatase, glutamate dehydrogenase, cholesterol, insulin, glucose, triglycerides). This suggested that MLKL was not contributing to development of NASH in this model (Figure 3A-C, Supplementary

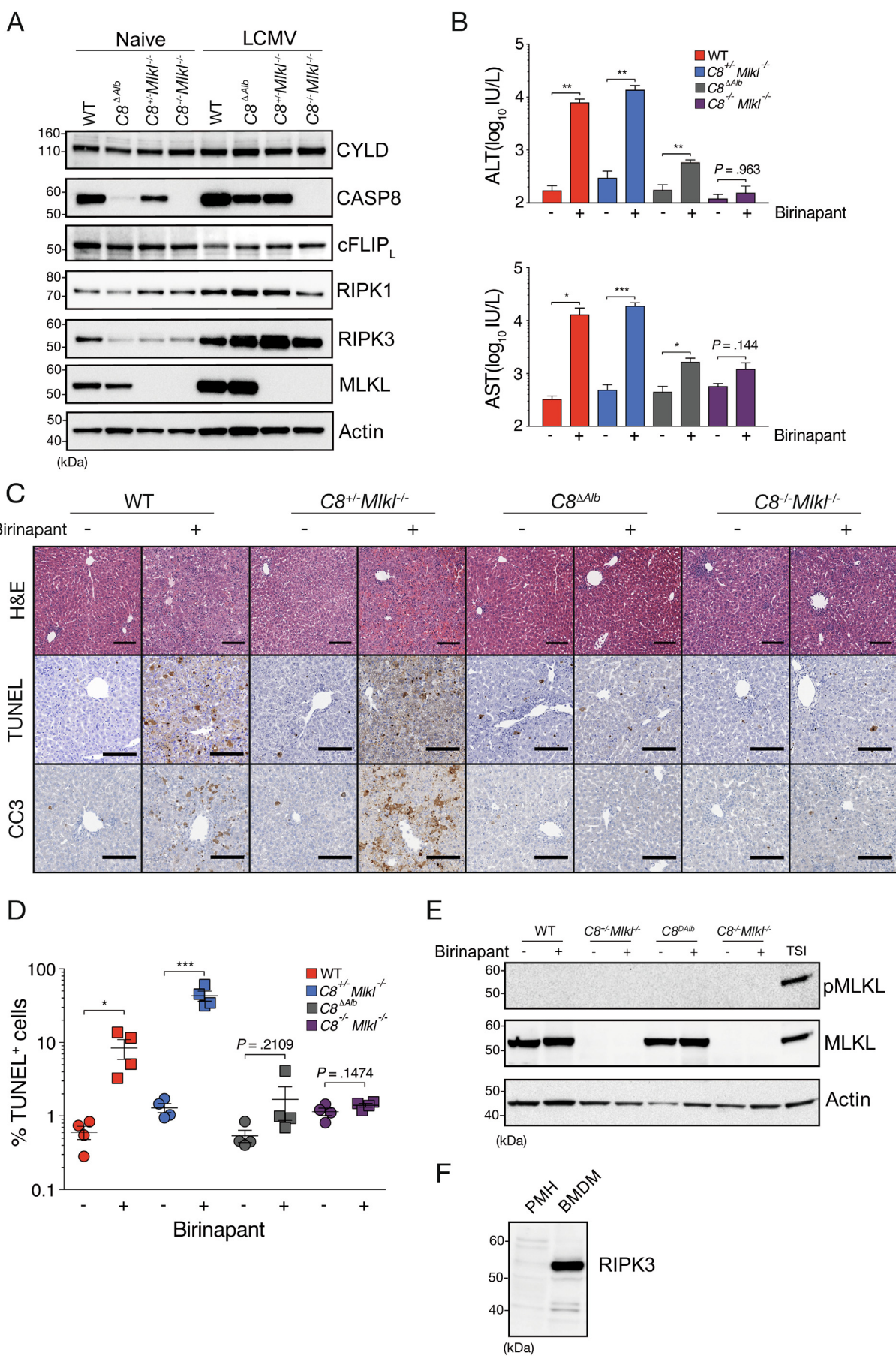
Figure 4A-K). Histological preparations from all animals fed CDAHFD showed numerous fat-filled hepatocytes and strong Sirius Red staining of collagen consistent with fibrotic and fatty liver disease (Figure 3D). Steatohepatitis based on NAFLD activity score (NAS) was similar between WT and MLKL-deficient mice (Figure 3E, Supplementary Figure 4L-O). We performed Western blots on whole liver lysates following 8 weeks of CDAHFD and did not detect phosphorylated (p)MLKL or (p)RIPK3 in any samples (Figure 3F).

Feeding mice with an HFD (60% kcal) is often referred to as the diet-induced obesity model of NAFLD. Both WT and MLKL-deficient animals fed HFD gained weight over 24 weeks. Similar to the CDAHFD model, there were no differences in total body, liver, or spleen weights or in adipose tissue and fat/lean composition, liver pathology, and serum ALT, AST, glutamate dehydrogenase, and alkaline phosphatase between genotypes following 24 weeks of HFD (Figure 3G-I and Supplementary Figure 5A-G). Glucose intolerance or insulin resistance are hallmarks of NAFLD in the diet-induced obesity model³⁸ and can be surrogate indicators of disease in obesity-related NAFLD/NASH. Importantly, both groups had similar basal glucose levels (Figure 3J) and we observed no differences in either glucose or insulin challenge tests across mouse genotypes (Supplementary Figure 5H and I). Liver histology using H&E, Sirius Red, and CC3 staining did not reveal differences in liver fat deposits, fibrosis, and apoptosis between genotypes (Figure 3K) after 24 weeks of HFD. Western blot analysis showed no activation/phosphorylation of RIPK3 or MLKL (Figure 3L), and RNAscope experiments could not detect expression of *Ripk3* messenger RNA (mRNA) in either WT or MLKL-deficient animals (Figure 3M). Together, these data indicate that necroptosis does not contribute to the progression of metabolic liver disease in the models we investigated.

Hepatocytes Restrict Activation of Necroptosis

Many cells undergo spontaneous necroptosis in the absence of caspase-8, but no liver abnormalities have been

Figure 3. Necroptosis does not contribute to the development and pathology associated with NAFLD or NASH in mice. (A-F) Male mice were fed either a normal diet (ND) or a choline-deficient high fat diet (CDAHFD, abbreviated to CFD) ad libitum for 8 weeks. (A) Weekly percentage change (D) from experimental start weight. (B) Whole mouse liver weight relative to total body weight and (C) ALT at 8 weeks postinfection. (D) Liver sections stained with H&E and Sirius Red. Scale bar 100 μm (H&E) or 500 μm (Sirius Red). (E) NAFLD Activity Score (NAS) (individual scoring values in supplementary data). (F) Western blot on whole liver lysates (n = 2 mice per dietary group and genotype). TSI are mouse WT BMDDMs treated with TNF, SMAC mimetic and caspase inhibitor QVD for 6 hours. Arrowheads indicate phosphorylated proteins. (G-M) Male mice were fed a 60% kcal HFD, containing choline. (G) Body weight was measured weekly for 24 weeks. (H) Total liver weight, (I) plasma ALT, and (J) basal glucose concentrations at the end of the experiment (n = 9–10 mice per group). (K) Liver sections stained with H&E, Sirius Red, or for CC3. Scale bar: 100 μm. (L) Western blot on whole liver lysates (n = 3 mice per dietary group and genotype). TS are mouse WT BMDDMs treated with TNF and SMAC mimetic for 6 hours, TSI described in Figure 3. Arrowheads indicate phosphorylated proteins (M) RNAscope for *Ripk3* mRNA on liver sections from WT and MLKL-deficient mice after 24 weeks. 3T3 (mouse) cells were used as positive control. Arrows indicate *Ripk3* mRNA specs. Scale bars: 100 μm, insert 50 μm. Data in (A-C, E) combined data from 4 independent experiments (total, n = 10–12). Images in (D) are representative of at least 10 to 12 histologic specimens. Data in (G-J) are combined data from 2 independent experiments (total, n = 9–10). Each symbol represents 1 mouse. Error bars represent SEM. *P < .05, **P < .005, ***P < .001, ****P < .0001 (A, 2-way analysis of variance [ANOVA] followed by a Tukey's multiple comparisons test compared ND and CDAHFD groups; B, C, and E, 1-way ANOVA followed by a Tukey's multiple comparisons test).



described in mice that lack caspase-8 specifically in hepatocytes (*C8^{ΔAlb}*).²⁸ In an attempt to forcibly drive necroptosis, we induced HBV infection in these gene-targeted mice. We have shown that this infection promotes MLKL protein expression in the liver (Figure 1A), and our previous work showed that HBV causes elevations in the death ligand TNF.³³ To bias the system even further toward necroptosis, we administered cIAP inhibitors (second mitochondria derived activator of caspases [SMAC] mimetics), which block nuclear factor- κ B survival signaling in hepatocytes and some cancer cells.³⁹ We saw 10- to 30-fold increases in serum AST and ALT levels in WT mice 6 hours following administration of the SMAC mimetic birinapant compared with vehicle-treated animals. In contrast, only minimally elevated plasma transaminase levels were detected in *C8^{ΔAlb}* and *C8^{-/-}Mlk1^{-/-}* mice (Supplementary Figure 6A and B). These data showed that the absence of caspase-8 was not promoting cell death but rather ameliorating it. We detected CC3- and TUNEL-positive cells in WT and *C8^{+/-}Mlk1^{-/-}* liver sections indicating that the elevations in transaminases and the cell death were due to the induction of apoptosis rather than necroptosis. Liver sections taken from experimentally treated *C8^{ΔAlb}* and *C8^{-/-}Mlk1^{-/-}* animals showed negligible cell death (Supplementary Figure 6C-E). The cell death we induced in the liver of infected mice promoted clearance of HBV and this was dependent on apoptosis, whereas necroptosis played no role (Supplementary Figure 6F). Collectively, these data showed that apoptosis can be induced in the liver, but necroptosis is restricted despite favorable and potent cell death conditions.

Necroptosis Is Prevented in Mouse Hepatocytes Despite Overwhelming Inflammation, Caspase-8 Loss and cIAP Inhibition

We conducted similar experiments using systemic and highly inflammatory LCMV, which causes increased protein expression of MLKL and RIPK3 (Figures 1A and 4A) in the liver, likely due to nonparenchymal cells, such as Kupffer cells and infiltrating T cells during infection (Supplementary Figure 7A).³ *C8^{ΔAlb}* mice were infected with LCMV Docile and treated with birinapant at the peak of the inflammatory and immunological response. Remarkably, compared to WT animals, *C8^{ΔAlb}* and *C8^{-/-}Mlk1^{-/-}* mice showed nominal hepatic damage, as determined by serum AST and ALT levels (Figure 4B). In contrast to WT animals, only minimal CC3 staining was noted in *C8^{ΔAlb}* and *C8^{-/-}Mlk1^{-/-}* mice

(Figure 4C-E and Supplementary Figure 7B). CC3 staining was concordant with TUNEL positivity, a nonspecific marker of cell death, indicating that apoptosis was responsible for cell death in this experimental model and we were unable to induce necroptosis. Some nonparenchymal cell apoptosis contributed to low-level TUNEL and CC3 staining in *C8^{ΔAlb}* animals (Supplementary Figure 7C and D).

Despite creating an *in vivo* hepatic milieu that highly favors the induction of necroptosis, we were unable to induce this form of cell death in the livers of animals. We confirmed this, by showing an absence of phosphorylated (p)MLKL in liver lysates (Figure 4E). Despite the presence of MLKL and RIPK3 in whole liver lysates, we hypothesized that hepatocytes do not express RIPK3. Western blot analysis on lysates from primary mouse hepatocytes and primary mouse bone marrow-derived macrophages (BMDM) confirmed that mouse hepatocytes did not express RIPK3 (Figure 4F).

Resistance to Necroptosis Is Conserved in Human Hepatocytes

We next investigated if the inability of liver cells to undergo necroptosis was conserved across mouse and human hepatocytes. Primary human peripheral blood mononuclear cells died in conditions that favored both apoptosis (TS) and necroptosis (TSQ), whereas primary human hepatocytes (PHH) were only susceptible to apoptosis (Figure 5A and B). We hypothesized that a relative deficiency of RIPK3 protein expression restricted hepatocyte necroptosis. We co-cultured PHH with a range of different stimuli that have been published as enhancing the expression of RIPK3 in PHHs or shown to induce RIPK3 expression in other cell types.^{18,35,40,41} Human RIPK3 protein was not detected in any conditions (Supplementary Figure 8A).

To examine if our *in vitro* findings were translatable to human hepatocytes *in vivo*, we used mice with chimeric human/mouse livers (HuLiver mice). *Fah^{-/-}Rag2^{-/-}Ii2ry^{-/-}* (FRG) mice had their livers repopulated with purified primary human hepatocytes.⁴² As these mice are *Fah* deficient, human hepatocytes can be identified using immunohistochemistry to stain for FAH. Three independent donors were used to generate mice and we confirmed a chimerism level of 40% to 80% (Supplementary Figure 8B and C, bottom panel) and all mice in our studies had detectable human serum albumin (Supplementary Figure 8D and E). We infected HuLiver mice with LCMV Docile and treated them with birinapant \pm emricasan (a clinical-stage inhibitor of caspase-8, also

Figure 4. Necroptosis is restricted in mouse hepatocytes *in vivo* even under highly inflammatory conditions. (A) Whole-liver lysates from mice of the indicated genotypes and conditions were analyzed by Western blot. LCMV-infected mice of mixed gender were taken 8 days post infection. (B) Serum ALT (top) and AST (bottom) measurements from LCMV-infected mice (day 8) 16 hours after treatment with birinapant (+) or vehicle (-) (n = 4). (C) Representative histologic liver H&E, TUNEL, or CC3 sections from experiment shown in (B). Scale bar: 125 μ m. (D) Quantification of TUNEL⁺ cells in the liver from experiment in (B and C). (E) Western blot performed on whole-liver lysates taken from the indicated mice from the experiment in (B and C). TSI is the lysate from RAW cells treated with TNF, SMAC mimetic and (caspase) Inhibitor (positive control). (F) Western blot performed on lysates from pure populations of primary mouse hepatocytes (PMH) or primary bone marrow derived macrophages (BMDM). Data are representative of 2 independent experiments with similar results (A-E). Error bars represent SEM. *P < .05, **P < .005, ***P < .001 (B and C, unpaired t-test; E, u-test).

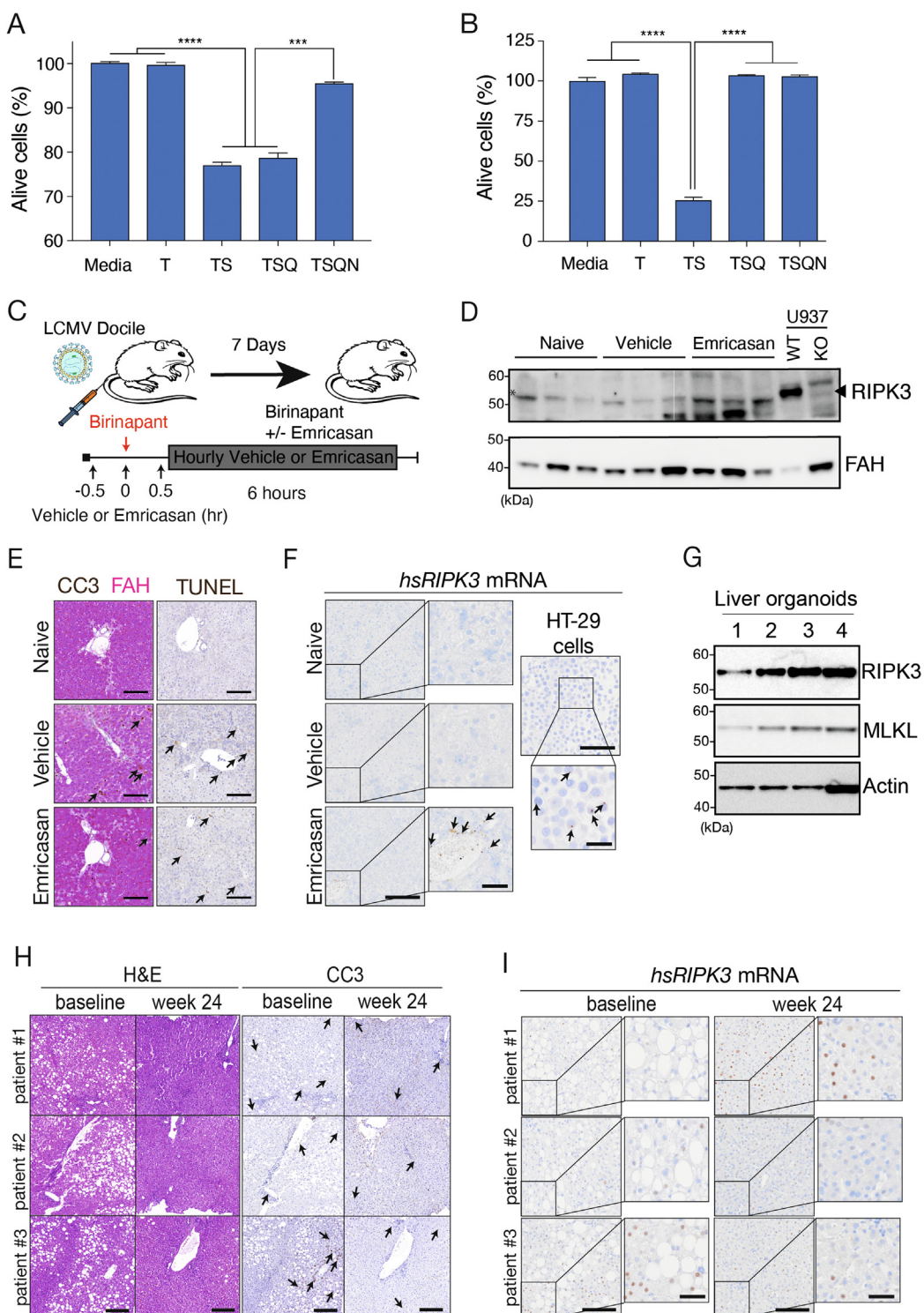
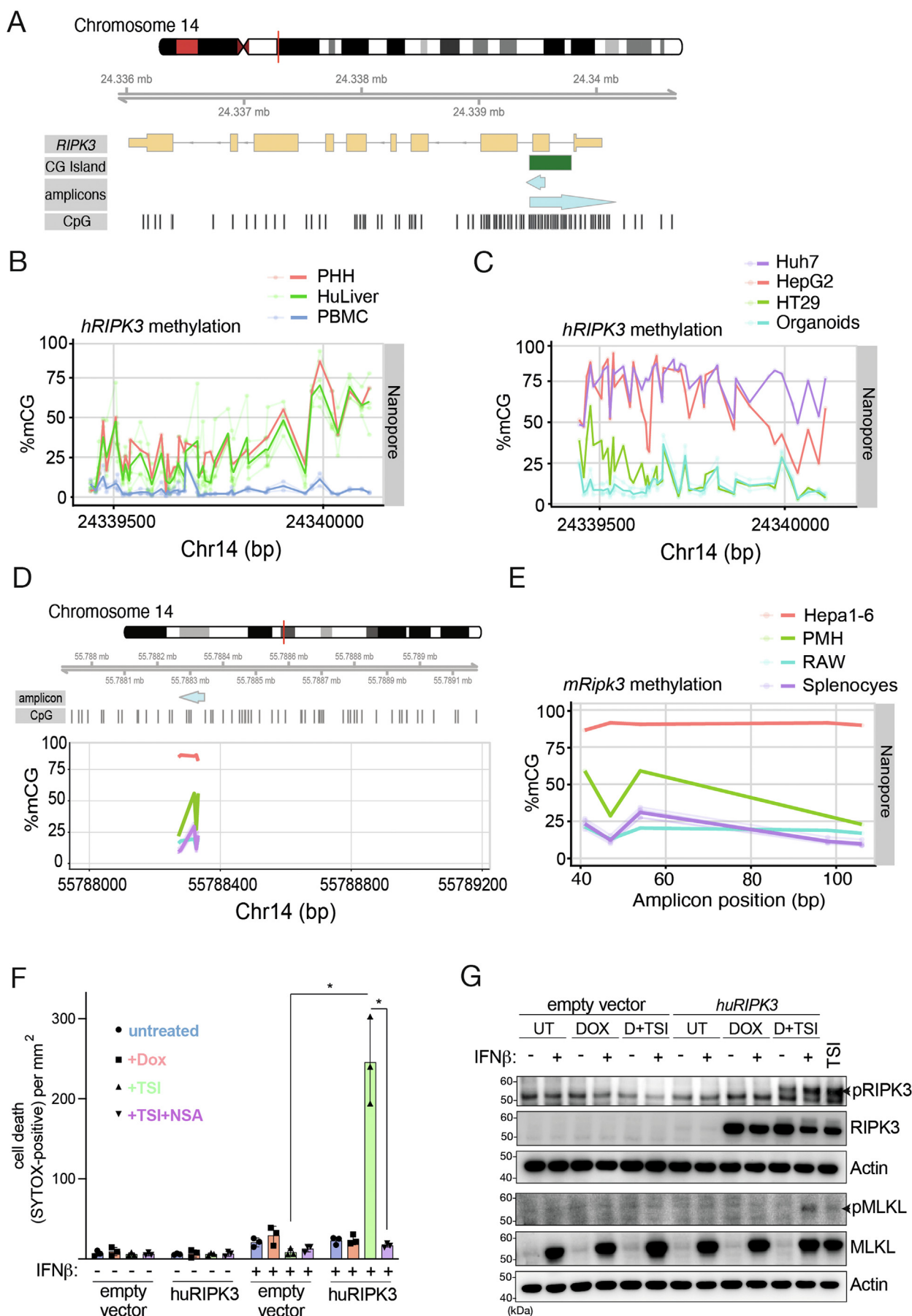


Figure 5. Primary human hepatocytes fail to undergo necroptosis in vitro and in vivo. (A) Human peripheral blood mononuclear cells or (B) PHHs were co-cultured with the indicated compounds and viability was measured. (C) Schematic indicating the experiment performed with HuLiver mice. Mice were infected with LCMV Docile 7 days before administration of birinapant and vehicle/emricasan. (D) Western blot analysis performed on whole-liver lysates from HuLiver mice and the relevant controls. * indicates a nonspecific band. Arrows indicate the correct band size of RIPK3. (E and F) Representative liver sections taken from HuLiver mice under the indicated conditions. (E) FAH (pink) and apoptotic death (CC3; brown; top) or total cell death (TUNEL; bottom). Arrows indicate hepatocytes positively stained for CC3 or TUNEL. (F) RNAscope analysis. Arrows indicate immune and HT-29 cells positively stained for human *RIPK3* mRNA probes. Scale bar: 100 μ m, insert 50 μ m. (G) Western blots performed on primary human liver organoids ($n = 4$). (H) Liver sections from 3 human patients with NASH at baseline and 24 weeks after dietary intervention, stained with H&E or for CC3. (I) RNAscope analysis of representative liver sections as in (H). Scale bar: 100 μ m, insert 50 μ m. Data in (A and B) are represented as the proportion of alive cells relative to untreated (Media). Data shown are representative of 3 independent experiments performed with similar results (A and B). FAH, fumarylacetoacetate hydrolase; N, necrostatin-1; Q, QVD-OPh; S, SMAC mimetic; T, TNF. *** $P = .0001$, **** $P < .0001$ (A and B, unpaired t -test; G, 1-way analysis of variance followed by a Tukey's multiple comparisons test).



known as IDN-6556) (Figure 5C). We were unable to detect RIPK3 in any of the 9 humanized mouse liver lysates (Figure 5D). We ensured that our antibody was able to specifically detect human RIPK3 and used the human monocytic cell line U937, as well as *RIPK3*^{-/-} U937 as positive and negative controls. A faint, nonspecific band was present on Western blots that could easily be mistaken for a RIPK3 band if these controls were not included in the analyses. This may explain why other groups have suggested that RIPK3 is expressed in human hepatocytes. Results from HuLiver mice infected with LCMV Docile and treated with birinapant ± emricasan were concordant with the results obtained in gene-targeted C57BL/6J mice described previously (Figure 5E and Supplementary Figure 8F). We performed RNAscope analysis and could not detect any mRNA expression of *RIPK3* in hepatocytes of HuLiver mice, only in infiltrating immune cells (Figure 6F).

Next, we generated and interrogated human liver organoids. Unlike the primary human hepatocytes (Figure 5D and Supplementary Figure 8A), these organoids all expressed the necroptotic mediators RIPK3 and MLKL (Figure 5G). However, we were not able to consistently induce necroptosis in organoids across different donors (Supplementary Figure 8G). This may reflect incomplete maturation or differentiation of hepatic-origin organoid stem cells into mature hepatocytes.

To confirm the human relevance of our mouse NAFLD and NASH data (see Figure 3), we collected paired liver biospecimen sections from 3 patients with NASH at baseline and at 24 weeks after dietary intervention. Histology analysis using H&E and Sirius Red revealed the typical features of NASH including liver ballooning and fibrosis, which regressed after dietary intervention (Supplementary Figure 8H). CC3 staining identified apoptotic hepatocytes in NASH specimens, confirming apoptosis as likely contributing to NASH pathophysiology (Figure 5H). RNAscope was used to assess transcriptional expression of *RIPK3*. We noted some pan-nuclear background staining in a few cells (Figure 5I) but we did not detect any specific cytoplasmic speckling that is characteristic of true translationally competent ribosomal transcripts (see Figure 5F, HT-29 cells, and Figure 3M, 3T3 cell for positive control). This was in keeping with our inability to identify RIPK3 protein in primary human

hepatocytes (Supplementary Figure 8A). We further explored why mouse and human hepatocytes do not reliably express RIPK3.

RIPK3 Is Epigenetically Silenced in Human and Mouse Hepatocytes

RIPK3 protein is undetectable in some primary tumors and several cancer cell lines because of the DNA hypermethylation of the promoter region of *RIPK3*, associated with gene silencing and transcriptional repression.^{23,24,43} However, it is unknown if the restricted expression of RIPK3 across primary, noncancerous cells such as hepatocytes could be due to epigenetic regulation. We identified an ~600 base pair region at the start of the human *RIPK3* gene that was rich in CpG dinucleotides, referred to as a CG island (CGI) (Figure 6A). High-throughput amplicon bisulfite sequencing of human DNA isolated from the livers of the HuLiver mice and one cryo-preserved primary human hepatocyte donor obtained commercially revealed that the CpG dinucleotides were hypermethylated in hepatocytes compared with primary peripheral blood mononuclear cell DNA from healthy donors (Figure 6B). Interestingly, we observed hypomethylation throughout the *RIPK3* CGI in liver organoid samples (Figure 6C), which was similar to that of HT-29 cells, a well-known colon adenocarcinoma cell line that is widely used to investigate necroptosis due to their expression of RIPK3 and MLKL^{16,44,45} (Figure 6C). This was consistent with the expression of RIPK3 protein in the liver organoids and may explain their ability to undergo necroptosis, which we speculated could reflect a degree of incomplete maturation (Figure 5F). We furthermore confirmed hypermethylation of this *RIPK3* CGI in 2 commonly used human hepatocyte cell lines, HepG2 and Huh7, as well as hypermethylation of *Ripk3* in primary mouse hepatocytes and the mouse liver cell line Hepa1–6, compared with hematopoietic primary splenocytes or a mouse macrophage cell line (RAW), consistent with a lack of RIPK3 expression in these cells²³ (Figure 6D and E).

To understand if the repression of RIPK3 in hepatocytes was responsible for the inability to undergo necroptosis, we used a lentiviral doxycycline inducible expression system to enforce expression of RIPK3 in Huh7 cells. Only in cells forced to express RIPK3 did we observe cell death. This was blocked with the human-specific, covalent MLKL-inhibitor

Figure 6. Epigenetic regulation of RIPK3 prevents necroptosis in human and mouse hepatocytes and necroptotic cell death can be restored by RIPK3 overexpression. (A–C) DNA methylation of the CpG island within the human *RIPK3* gene. (A) Schematic indicating the position of gene components and amplicons used for methylation sequencing of the human *RIPK3* gene, located on chromosome 14. DNA was isolated from the indicated human sources: (B) PHHs n = 1, HuLiver n = 5, peripheral blood mononuclear cell n = 3. (C) Organoids (n = 4) (samples were the same as those used in Figure 7F and Supplementary Figure 5G), HepG2 (n = 1), HT29 (n = 1), Huh7 (n = 1). **Bold lines** indicate the mean methylation and **thin lines** indicate individual donors. (D and E) Nanopore amplicon bisulfite sequencing performed on DNA from primary C57BL/6 mouse splenocytes (n = 5), cryopreserved primary mouse hepatocytes (PMH) (n = 1), RAW cells (n = 1), and Hepa1–6 cells (n = 1). **Solid lines** indicate the mean methylation. **Translucent lines** indicate individual donors. (F and G) IncuCyte cell death assay and Western blot of Huh7 cells transduced with a dox-inducible lentiviral expression vector encoding human *RIPK3* (or empty vector control) and treated with the indicated stimuli ± interferon (IFN)β. Cell death in (F) was measured by SYTOX uptake. *P < .05 (unpaired t-test with Welch's correction). Western blot (G) was performed on whole cell lysates taken at 6 hours post treatment. TSI (positive control) as in previous figures. Arrowheads indicate bands showing phosphorylated proteins.

necrosulfonamide, confirming that the type of cell death was necroptosis and driven solely by induction of RIPK3 expression (Figure 6F). We confirmed RIPK3 and MLKL activation/phosphorylation by Western blot analysis (Figure 6G). Collectively, our work supports the notion that hepatocytes from both mice and humans transcriptionally repress RIPK3 and prevent necroptosis.

Discussion

In addition to its essential role in necroptosis, RIPK3 has more recently been implicated in inflammation signaling.^{46,47} This has made us revisit many studies that used RIPK3-deficient mice to implicate necroptosis in disease processes. It is now clear that such studies could be confounded by RIPK3's non-necroptotic roles. It is also important to note that studies examining RIPK3 function in certain cells and tissues may not be generalizable to all organs as RIPK3 is not ubiquitously expressed. Although some groups have reported both expression and a critical role for RIPK3 in hepatocytes,^{4,35,48} we and others²⁵ have shown that RIPK3 protein expression is not detectable in hepatocytes. The unavailability of specific antibodies at the time of these studies and the presence of RIPK3 in non-hepatic parenchymal cells such as Kupffer cells may be responsible for the disparity in results.

Collectively our MLKL and RIPK3 data are consistent with the notion that necroptosis is repressed in hepatocytes and does not contribute to the liver pathologies we have studied. In all of our experiments, we controlled for genetic background, housing conditions, and environment. We used littermate controls, sex-matched cohorts, and housed experimental animals in identical conditions. Given our data showing that expression of RIPK3 is repressed in hepatocytes and our data showing identical hepatic phenotypes in MLKL-deficient and WT mice, it is difficult to implicate these molecules in liver disease. Both RIPK3 and MLKL are present in Kupffer cells, and it is plausible that detection of these molecules in hemopoietic cells may have confounded interpretation of results using whole liver lysates.

Interestingly, the hypermethylation of the *RIPK3* promoter in human DNA from PHHs and hepatocytes harvested from HuLiver mice contrasted with the hypomethylation observed in human liver organoids, which displayed variability in their capacity to undergo necroptosis. This again contrasted with the complete block in necroptosis observed *in vitro*, *ex vivo*, and *in vivo* in adult and mouse liver tissue. We speculate that the inconsistencies between hepatocyte organoid data and true adult hepatocyte data could be due to incomplete maturation or differentiation of hepatocyte organoid stem cells. It is generally accepted that although liver organoids are a reasonable representation of liver tissue, they do not reflect all the nuances of fully differentiated adult liver. For example, during differentiation and development they are not exposed to the same *in vivo* ontological cues that may affect epigenetic silencing of signaling pathways and additionally *in vitro* cues or selection pressures may cause the inactivation of certain pathways through diverse mechanisms that are not reflected

in vivo. Hence, our organoid data need to be interpreted with caution and experiments that exclusively use liver organoids to make assumptions about necroptosis and its relevance to human disease need to be treated with the same caution.

We clearly showed that *RIPK3* mRNA is repressed or at least not overtly expressed across paired human NASH biospecimens collected before and after dietary intervention. The latter specimens showed regression of pathology. Phosphorylated MLKL is essential for necroptosis, but not sufficient, and we did not detect phosphorylated MLKL in liver lysates from our mouse models of metabolic liver disease. In mice infected with LCMV, in which antiviral responses lead to immune cell infiltration, we did not detect *Ripk3* transcripts in hepatocytes but we did detect these transcripts in the infiltrating immune cells. Importantly, we have shown that complete absence of MLKL in mice does not ameliorate any of the diseases we have studied, including 2 mouse models of diet-induced liver disease.

It is interesting to speculate why hepatocytes repress RIPK3 expression. It is well established that RIPK3 is involved in processes outside of necroptosis.⁴⁷ Perhaps RIPK3 is hepatically repressed not to prevent necroptosis but to interrupt other RIPK3-dependent processes that could be deleterious to the host, including excessive inflammation. Our finding that *RIPK3* is epigenetically silenced in primary hepatocytes, affecting their ability to undergo necroptosis, is an important finding in the gastroenterology field.

Supplementary Material

Note: To access the supplementary material accompanying this article, visit the online version of *Gastroenterology* at www.gastrojournal.org, and at <http://doi.org/10.1053/j.gastro.2022.08.040>.

References

1. Luedde T, Kaplowitz N, Schwabe RF. Cell death and cell death responses in liver disease: mechanisms and clinical relevance. *Gastroenterology* 2014;147:765–783.e4.
2. Schwabe RF, Luedde T. Apoptosis and necroptosis in the liver: a matter of life and death. *Nat Rev Gastroenterol Hepatol* 2018;93:101.
3. Dara L, Liu Z-X, Kaplowitz N. Questions and controversies: the role of necroptosis in liver disease. *Cell Death Discov* 2016;2:16089.
4. Gautheron J, Vucur M, Luedde T. Necroptosis in non-alcoholic steatohepatitis. *Cell Mol Gastroenterol Hepatol* 2015;1:264–265.
5. Aron-Wisnewsky J, Vigliotti C, Witjes J, et al. Gut microbiota and human NAFLD: disentangling microbial signatures from metabolic disorders. *Nat Rev Gastroenterol* 2020;17:279–297.
6. Holler N, Zarz R, Micheau O, et al. Fas triggers an alternative, caspase-8-independent cell death pathway using the kinase RIP as effector molecule. *Nat Immunol* 2000;1:489–495.

- HEPATOBILIARY**
7. He S, Liang Y, Shao F, et al. Toll-like receptors activate programmed necrosis in macrophages through a receptor-interacting kinase-3-mediated pathway. *Proc Natl Acad Sci U S A* 2011;108:20054–20059.
 8. Jouan-Lanhouet S, Arshad MI, Piquet-Pellorce C, et al. TRAIL induces necroptosis involving RIPK1/RIPK3-dependent PARP-1 activation. *Cell Death Differ* 2012;19:2003–2014.
 9. Newton K, Manning G. Necroptosis and inflammation. *Annu Rev Biochem* 2016;85:743–763.
 10. Samson AL, Garnish SE, Hildebrand JM, et al. Location, location, location: a compartmentalized view of TNF-induced necroptotic signaling. *Sci Signal* 2021;14:eabc6178.
 11. Murphy JM. The killer pseudokinase mixed lineage kinase domain-like protein (MLKL). *Cold Spring Harb Perspect Biol* 2019;12:a036376.
 12. Tummers B, Green DR. Caspase-8: regulating life and death. *Immunol Rev* 2017;277:76–89.
 13. Feng S, Yang Y, Mei Y, et al. Cleavage of RIP3 inactivates its caspase-independent apoptosis pathway by removal of kinase domain. *Cell Signal* 2007;19:2056–2067.
 14. Hildebrand JM, Tanzer MC, Lucet IS, et al. Activation of the pseudokinase MLKL unleashes the four-helix bundle domain to induce membrane localization and necroptotic cell death. *Proc Natl Acad Sci U S A* 2014;111:15072–15077.
 15. Samson AL, Fitzgibbon C, Patel KM, et al. A toolbox for imaging RIPK1, RIPK3, and MLKL in mouse and human cells. *Cell Death Differ* 2021;28:2126–2144.
 16. Samson AL, Zhang Y, Geoghegan ND, et al. MLKL trafficking and accumulation at the plasma membrane control the kinetics and threshold for necroptosis. *Nat Commun* 2020;11:3151.
 17. Murphy JM, Czabotar PE, Hildebrand JM, et al. The pseudokinase MLKL mediates necroptosis via a molecular switch mechanism. *Immunity* 2013;39:443–453.
 18. Stutz MD, Ojaimi S, Allison C, et al. Necroptotic signaling is primed in *Mycobacterium tuberculosis*-infected macrophages, but its pathophysiological consequence in disease is restricted. *Cell Death Differ* 2018;25:951–965.
 19. Sarhan J, Liu BC, Muendlein HI, et al. Constitutive interferon signaling maintains critical threshold of MLKL expression to license necroptosis. *Cell Death Differ* 2019;26:332–347.
 20. Knuth A-K, Rösler S, Schenk B, et al. Interferons transcriptionally up-regulate MLKL expression in cancer cells. *Neoplasia* 2019;21:74–81.
 21. Sai K, Parsons C, House JS, et al. Necroptosis mediators RIPK3 and MLKL suppress intracellular Listeria replication independently of host cell killing. *J Cell Biol* 2019;218:1994–2005.
 22. Rickard JA, O'Donnell JA, Evans JM, et al. RIPK1 regulates RIPK3-MLKL-driven systemic inflammation and emergency hematopoiesis. *Cell* 2014;157:1175–1188.
 23. Koo G-B, Morgan MJ, Lee D-G, et al. Methylation-dependent loss of RIP3 expression in cancer represses programmed necrosis in response to chemotherapeutics. *Cell Res* 2015;25:707–725.
 24. Yang C, Li J, Yu L, et al. Regulation of RIP3 by the transcription factor Sp1 and the epigenetic regulator UHRF1 modulates cancer cell necroptosis. *Cell Death Dis* 2017;8:e3084.
 25. Dara L, Johnson H, Suda J, et al. Receptor interacting protein kinase 1 mediates murine acetaminophen toxicity independent of the necosome and not through necroptosis. *Hepatology* 2015;62:1847–1857.
 26. Günther C, He G-W, Kremer AE, et al. The pseudokinase MLKL mediates programmed hepatocellular necrosis independently of RIPK3 during hepatitis. *J Clin Investig* 2016;126:4346–4360.
 27. Alvarez-Diaz S, Dillon CP, Lalaoui N, et al. The pseudokinase MLKL and the kinase RIPK3 have distinct roles in autoimmune disease caused by loss of death-receptor-induced apoptosis. *Immunity* 2016;45:513–526.
 28. Kaufmann T, Jost PJ, Pellegrini M, et al. Fatal hepatitis mediated by tumor necrosis factor $TNF\alpha$ requires caspase-8 and involves the BH3-only proteins Bid and Bim. *Immunity* 2009;30:56–66.
 29. Preston SP, Pellegrini M, Ebert G. Hydrodynamic injection as a method of gene delivery in mice: a model of chronic hepatitis B virus infection. *Methods Mol Biol* 2016;1419:109–115.
 30. Armistead JS, Jennison C, O'Neill MT, et al. *Plasmodium falciparum* subtilisin-like ookinete protein SOPT plays an important and conserved role during ookinete infection of the *Anopheles stephensi* midgut. *Mol Microbiol* 2018;109:458–473.
 31. Dillon CP, Weinlich R, Rodriguez DA, et al. RIPK1 blocks early postnatal lethality mediated by caspase-8 and RIPK3. *Cell* 2014;157:1189–1202.
 32. Afonso MB, Rodrigues PM, Carvalho T, et al. Necroptosis is a key pathogenic event in human and experimental murine models of non-alcoholic steatohepatitis. *Clin Sci (Lond)* 2015;129:721–739.
 33. Ebert G, Preston S, Allison C, et al. Cellular inhibitor of apoptosis proteins prevent clearance of hepatitis B virus. *Proc Natl Acad Sci U S A* 2015;112:5797–5802.
 34. Yang ASP, Boddey JA. Molecular mechanisms of host cell traversal by malaria sporozoites. *Int J Parasitol* 2017;47:129–136.
 35. Gautheron J, Vucur M, Reisinger F, et al. A positive feedback loop between RIP3 and JNK controls non-alcoholic steatohepatitis. *EMBO Mol Med* 2014;6:1062–1074.
 36. Heintz MM, McRee R, Kumar R, et al. Gender differences in diet-induced steatotic disease in Cyp2b-null mice. *PLoS One* 2020;15:e0229896.
 37. Albaisi SAM, Bajaj JS. The influence of the microbiome on NAFLD and NASH. *Clin Liver Dis* 2021;17:15–18.
 38. Karunakaran D, Turner AW, Duchez A-C, et al. RIPK1 gene variants associate with obesity in humans and can be therapeutically silenced to reduce obesity in mice. *Nat Metab* 2020;2:1113–1125.
 39. Ebert G, Allison C, Preston S, et al. Eliminating hepatitis B by antagonizing cellular inhibitors of apoptosis. *Proc Natl Acad Sci U S A* 2015;112:5803–5808.

40. Roychowdhury S, McMullen MR, Pisano SG, et al. Absence of receptor interacting protein kinase 3 prevents ethanol-induced liver injury. *Hepatology* 2013; 57:1773–1783.
41. Wang S, Ni H-M, Dorko K, et al. Increased hepatic receptor interacting protein kinase 3 expression due to impaired proteasomal functions contributes to alcohol-induced steatosis and liver injury. *Oncotarget* 2016;7:17681–17698.
42. Azuma H, Pault N, Ranade A, et al. Robust expansion of human hepatocytes in *Fah*^{−/−}/*Rag2*^{−/−}/*Il2rg*^{−/−} mice. *Nat Biotechnol* 2007;25:903–910.
43. Yang Z, Jiang B, Wang Y, et al. 2-HG inhibits necroptosis by stimulating DNMT1-dependent hypermethylation of the RIP3 promoter. *Cell Rep* 2017; 19:1846–1857.
44. Meng Y, Davies KA, Fitzgibbon C, et al. Human RIPK3 maintains MLKL in an inactive conformation prior to cell death by necroptosis. *Nat Commun* 2021;12:6783.
45. Garnish SE, Meng Y, Koide A, et al. Conformational interconversion of MLKL and disengagement from RIPK3 precede cell death by necroptosis. *Nat Commun* 2021; 12:2211.
46. Daniels BP, Snyder AG, Olsen TM, et al. RIPK3 restricts viral pathogenesis via cell death-independent neuroinflammation. *Cell* 2017;169:301–313.e11.
47. Moriwaki K, Chan FKM. The inflammatory signal adaptor RIPK3: functions beyond necroptosis. *Int Rev Cell Mol Biol* 2017;328:253–275.
48. Roychowdhury S, McCullough RL, Sanz-Garcia C, et al. Receptor interacting protein 3 protects mice from high-fat diet-induced liver injury. *Hepatology* 2016;64:1518–1533.

Author names in bold designate shared co-first authorship.

Received September 13, 2021. Accepted August 16, 2022.

Correspondence

Address correspondence to Marc Pellegrini, MD, PhD, and Marcel Doerflinger, PhD, Walter and Eliza Hall Institute of Medical Research, 1G Royal Parade, Parkville 3052, Victoria, Australia. e-mail: Pellegrini@wehi.edu.au or doerflinger.m@wehi.edu.au.

Acknowledgments

We thank Warren Alexander, Razqallah Hakem, and Stephen Hedrick for mice. Pei-Jer Chen and Ding-Shinn Chen constructed the hepatitis B virus vector for hydrodynamic injection. John Silke provided the *RIPK3*^{−/−} U937 cell line. Carolina Alvarado, Kristy Vella, and Merle Dayton provided excellent animal husbandry and Sara Erickson provided valuable insectary support. We thank Andre Samson, Destiny Dalseno, Emma Pan, and Ellen Tsui for expert advice and help with RNAScope experiments. We acknowledge scholarship support for Yanxiang Meng (Melbourne Research Scholarship, AINSE PGRA scholarship). We also thank the Walter and Eliza Hall histology and imaging departments for their services, along with Ms Yizhuo Wang, Ms Xichun (Shirley) Li, and The University of Queensland Biological Resources (UQBR), for technical assistance.

CRedit Authorship Contributions

Order of Authors (with Contributor Roles):

Simon P. Preston, PhD (Conceptualization: Supporting; Formal analysis: Lead; Investigation: Lead; Methodology: Lead; Writing – original draft: Lead; Writing – review & editing: Equal).

Michael D. Stutz, PhD (Investigation: Supporting; Methodology: Supporting).

Cody C. Allison, PhD (Investigation: Supporting; Methodology: Supporting).

Ueli Nachbur, PhD (Conceptualization: Supporting; Investigation: Supporting; Methodology: Supporting).

Quentin Gouil, PhD (Conceptualization: Supporting; Investigation: Supporting; Methodology: Supporting).

Bang Manh Tran, PhD (Investigation: Supporting).

Valerie Duvivier, PhD (Conceptualization: Supporting; Investigation: Supporting; Methodology: Supporting).

Philip Arandjelovic, PhD (Investigation: Supporting).

James Cooney, PhD (Investigation: Supporting).

Liana Mackiewicz, DipAnH (Investigation: Supporting).

Yanxiang Meng, PhD (Data curation: Supporting; Formal analysis: Supporting).

Jan Schaefer, MSc (Data curation: Supporting).

Stefanie M. Bader, MSc (Data curation: Supporting).

Hongke Peng, PhD (Investigation: Supporting).

Zina Valaydon, MD, PhD (Investigation: Supporting; Methodology: Supporting).

Pravin Rajasekaran, PhD (Investigation: Supporting).

Charlie Jennison, PhD (Investigation: Supporting).

Sash Lopaticki, BSci (Investigation: Supporting).

Ann Farell, PhD (Data curation: Supporting; Resources: Supporting).

Marni Ryan, MD (Resources: Supporting; Supervision: Supporting).

Jessica Howell, PhD (Data curation: Supporting; Resources: Supporting; Supervision: Supporting).

Catherine Croagh, MD (Data curation: Supporting; Resources: Supporting; Supervision: Supporting).

Denuja Karunakaran, PhD (Investigation: Supporting).

Carole Schuster-Klein, PhD (Conceptualization: Supporting; Methodology: Supporting).

James M. Murphy, PhD (Conceptualization: Supporting).

Theodora Fifis, PhD (Conceptualization: Supporting).

Christopher Christophi, MD PhD (Conceptualization: Supporting).

Elizabeth Vincan, PhD (Conceptualization: Supporting).

Alexander Thompson, MD, PhD (Investigation: Supporting; Resources: Supporting; Supervision: Supporting).

Marnie E. Blewitt, PhD (Conceptualization: Supporting; Methodology: Supporting).

Justin A. Boddey, PhD (Conceptualization: Supporting; Methodology: Supporting).

Marcel Doerflinger, PhD (Conceptualization: Supporting; Investigation: Equal; Methodology: Supporting; Supervision: Supporting; Writing – review & editing: Equal).

Marc Pellegrini, MD, MB BS, BSc, PhD, FRACP, FAHMS (Conceptualization: Lead; Funding acquisition: Lead; Writing – review & editing: Equal).

Conflict of interest

Some funding was obtained from Les Laboratoires Servier and Anaxis Pharma. The authors disclose no conflicts.

Funding

Funding was provided by the following: National Health and Medical Research Council Australia grants 1139153 and 1123727 to Justin A. Boddey; 1194345 to Marnie E. Blewitt; 1172929 to James M. Murphy; 1181580 to Elizabeth Vincan and Bang Manh Tran; and 1006592, 1045549, and 1065626 to Marc Pellegrini. Melbourne Health grant PG-002-2016 to Elizabeth Vincan, Theodora Fifis, and Christopher Christophi. Bellberry-Viertel fellowship to Marnie E. Blewitt. Institute for Molecular Bioscience (IMB) Fellowship to Denuja Karunakaran. The Victorian State Government Operational Infrastructure Support and the Independent Research Institutes Infrastructure Support Scheme of the Australian Government National Health and Medical Research Council to the Walter and Eliza Hall Institute of Medical Research, Parkville, Victoria, Australia.

Supplementary Materials and Methods

Measurement of Serum Transaminase Levels, Albumin, and HBV Serology

Terminal bleeds were performed on euthanized mice and serum was separated from coagulated blood by centrifugation at 2000g. Activated AST, activated ALT, and human albumin (hALB) were quantified on the ARCHITECT cSystem (Abbott Laboratories, Chicago, IL) according to the manufacturer's instructions. Anti-hepatitis B surface antigen (anti-HBs) antibodies were quantified using a Cobas e411 analyzer (Roche, Basel, Switzerland) according to the manufacturer's instructions.

Parasites and Mosquito Infections

Swiss Webster mice infected with asexual *P. berghei* ANKA *PbGFP-Luc_{con}* were used for direct feeding assays.¹ Mice with 2% parasitemia and exhibiting exflagellation of microgametes by microscopy were anesthetized with ketamine/xylazine via intraperitoneal (IP) inoculation, and individually placed on top of a single container of 50 female *Anopheles stephensi* mosquitoes that were 3 to 5 days old. Mosquitoes fed on mice for 15 minutes, after which any unfed mosquitoes were collected and discarded.

NASH Model and Histological Scoring

Mlk1^{+/−} heterozygous C57BL/6 mice were intercrossed to generate littermates that were either WT for *Mlk1*, *Mlk1^{+/−}*, or *Mlk1^{−/−}*. Littermates were separated into cages based on genotype at weaning, and at 5 weeks of age were fed ad libitum either a normal diet (ND) (Mice breeder cube, Ridley, Melbourne, VIC, Australia) or a CDAHFD (SF17-107; Specialty Feeds, Glen Forest, WA, Australia; Research Diets A06071302 Equivalent) for 8 weeks. CDAHFD contains 0.1% methionine and 60% kcal fat. Only male mice were used for experiments. Blood parameters for NASH experiments were analyzed commercially (ASAP Laboratory, Mulgrave, VIC, Australia). Histologic scoring was performed by an expert pathologist on formalin-fixed paraffin-embedded liver sections. The pathologist was blinded to the mouse genotype and diet. Steatosis scoring: 0 < 5%; 1 = 5% to 33%; 2 = 34% to 66%; 3 > 66%. Lobular inflammation scoring: 0 = none; 1 < 2 loci; 2 = 2 to 4 loci; 3 > 4 loci. Fibrosis scoring: 0 = none; 1 = perisinusoidal or portal; 2 = perisinusoidal and portal; 3 = fibrotic septa; 4 = cirrhosis. The NAS scoring system was developed by the NASH clinical research network and is calculated by the sum of the steatosis, lobular inflammation, and fibrosis scoring described previously.² An NAS score of ≤ 3 is correlated with a diagnosis of "not NASH," whereas an NAS score of ≥ 5 is correlated with a diagnosis of "definitely NASH." Alternatively, mice were fed on a rodent diet with 60% kcal fat (HFD) (D12492; Research Diets Inc., New Brunswick, NJ). As described previously,³ mice were fasted for 6 hours and then received IP injections of 1 g kg^{−1} of D-glucose (Fisher Scientific) or 0.75 units per kg of insulin (HI0213, Eli Lilly). Blood parameters for NASH experiments

were analyzed commercially (ASAP Laboratory, Mulgrave, VIC, Australia). Blood glucose was measured from the tail vein at the depicted time intervals with an Accu-Chek Aviva Nano glucose meter (Roche). Blood glucose levels in each group were averaged and plotted for each time point, and the area under the curve was determined for each individual mouse. Western blots from whole liver lysates were performed as described in the following.

Drug Treatment

In vivo administration of SMAC mimetic (Birinapant; Tetralogic Pharmaceuticals, Malvern, PA) was delivered by IP injection at a dose of 30 mg/kg in a volume of 50 μL dimethyl sulfoxide (DMSO). The vehicle used was DMSO. Emricasan (also known as IDN-6556; MedKoo Biosciences, Chapel Hill, NC) was administered by intravenous (IV) or IP injection at a dose of 60 mg/kg in a volume of 100 μL diluted in vehicle. Vehicle contained 10% (vol/vol) DMSO, 2% Solutol (vol/vol) in 53 mM phosphate buffer pH 8.0.

Western Blots

Cells or tissue being analyzed by western blot were strictly kept on ice and were lysed in buffer containing 135 mM NaCl, 20 mM Tris-HCl (pH 7.5), 1.5 mM Mg₂Cl₁, 1 mM EGTA, 10% glycerol, 1% Triton X-100, protease, and phosphatase inhibitors (Roche). Alternatively, organoid cells were harvested by washing and centrifuging at 300g several times with ice-cold Dulbecco's modified Eagle's medium (DMEM) (Gibco, Waltham, MA; #11995073) until the BME2 matrix was completely removed. The cell pellets were then resuspended in 200 μL of 1X Passive Lysis Buffer (Promega, Madison, WI; #E1960) and incubated at room temperature for 20 minutes. Lysates were boiled for 5 minutes in sodium dodecyl sulfate (SDS) loading buffer and separated using 4% to 12% Bis-Tris pre-cast gels (ThermoScientific, Waltham, MA). Proteins were transferred onto nitrocellulose membranes (ThermoScientific) and detected using primary and secondary antibodies.

The following antibodies to detect mouse protein were used: rat anti-MLKL (3H1; available from Merck Millipore, Bedford, MA), rabbit anti-CYLD (D1A10; CST), rat anti-caspase-8 (1G12; WEHI), rat anti-cFLIP (Dave-2; Adipogen, San Diego, CA), mouse anti-RIPK1 (38/RIP; BD Biosciences, San Jose, CA), rabbit anti-RIP1 (D94C12) (CST), rabbit anti-p-RIP1 (Ser166) (CST), rabbit anti-RIPK3 (ProSci, Poway, CA), rabbit anti-p-MLKL (phospho S345) (EPR9515; Abcam, Cambridge, UK), and rabbit anti-p-RIPK3 (S232, T231) (Genentech, San Francisco, CA). The following antibodies to detect human protein were used: rabbit anti-FAH (ThermoFisher), rabbit anti-RIPK3 (E1Z1D; CST), rabbit anti-p-RIPK3 (ser227) D6W2T (CST), rat anti-MLKL 7G2 (WEHI), and rabbit anti-p-MLKL (Abcam ab187091).

All secondary antibodies used were from Southern Biotech (Birmingham, AL) and were all horseradish peroxidase (HRP) conjugated. For loading controls, rabbit anti-β actin (CST) or rabbit anti-β actin (HRP conjugate) (13E5; CST) were used. Controls for blots included lysates from WT human U937 cells, *RIPK3^{−/−}* U937 cells, mouse bone

marrow-derived macrophages (mBMDM), and WT mouse whole liver (mLiver). TS control for mouse samples was a lysate derived from mBMDMs treated for 6 hours with 100 ng/mL mouse tumor necrosis factor (TNF) (Biolegend, San Diego, CA), 10 μ M SMAC mimetic (Birinapant; Teralogic Pharmaceuticals, PA). TSI control for mouse samples was a lysate derived from mBMDMs or RAW macrophages and for human samples was a lysate derived from HT-29 samples treated for 6 to 9 hours with 100 ng/mL mouse TNF (Biolegend), 10 μ M SMAC mimetic (Birinapant; Teralogic Pharmaceuticals) and 40 μ M pan-caspase inhibitor QVD-OPh (Sigma-Aldrich, St. Louis, MO).

Liver Histology and Immunostaining

The left lateral lobe was removed from euthanized mice and immediately perfused with ice-cold phosphate-buffered saline (PBS) before fixation in 10% buffered formalin. Tissue sections were prepared from paraffin blocks and stained with H&E or Sirius Red or immunohistochemically with an *in situ* cell death kit (TUNEL; Abcam) or with antibodies recognizing: CC3 (R&D systems, Minneapolis, MN), CD3 (Agilent Technologies [Dako], Santa Clara, CA), CD8 (Synaptic Systems, Gottingen, Germany), F4/80 (WEHI), hepatitis B core antigen (HBcAg) (Agilent Technologies [Dako]), or FAH (ThermoFisher Scientific). RNAscope on mouse and human liver sections was performed using RNAscope 2.5 BROWN assay (ACD Biotech, Newark, CA) as per the manufacturer's instruction using probes specific for either mouse (cat# 462541) or human (cat# 434661) Ripk3 mRNA. We used paraffin-embedded pellets of 3T3 cells or HT-29 as controls for mouse or human assays, respectively.

Histologic slides were scanned using a Panoramic SCAN II scanner (3D Histech, Budapest, Hungary). Images were analyzed using FIJI⁴ with a custom written analysis pipeline that made use of the color deconvolution function to separate the stains into separate channels. A median filter was applied and each channel binarized using user-defined thresholds. Object counts were recorded and binary masks output for user verification. Because of the size of the files involved, each image was split into tiles for memory management and speed of processing. The object counts were summed across all tiles.

Enumeration of apoptotic bodies observed in histologic liver sections stained with H&E from HuLiver mice were performed by a pathologist.

Cytokine Measurement

Serum cytokine levels were determined using a Milliplex (Merck Millipore) multiplex cytokine assay. Results were determined using the Luminex 200 instrument (R&D systems) and data were analyzed using xPonent software.

Cell Culture and Death Assays

Peripheral blood mononuclear cells (PMBCs) were isolated from leukapheresed human blood taken from healthy donors (Australian Red Cross). Briefly, blood was mixed 1:2 with PBS and layered over 100% Ficoll Plus (GE Healthcare, Chicago, IL) and centrifuged at 400g for 30 minutes at room

temperature without brake. The buffy layer, containing PMBCs, was washed 5 times with cold PBS by centrifugation at 250g for 10 minutes at 4°C. PMBCs were resuspended in RPMI-GlutaMAX (ThermoFisher Scientific) supplemented with 10% fetal calf serum (FCS), penicillin-streptomycin and 50 μ M 2-mercaptoethanol. PMBCs were seeded in triplicate in 24-well plates at a density of 1.25×10^6 cells/well and rested for 4 hours. Cells were treated with combinations of 40 μ M QVD-OPh (Sigma-Aldrich) and 60 μ M necrostatin-1 (Enzo Life Sciences, Farmingdale, NY) 1 hour before addition of 100 ng/mL recombinant TNF (Biolegend) and 10 μ M SMAC mimetic (Birinapant; Teralogic Pharmaceuticals). After 24 hours, cells were harvested and propidium iodide-positive cells (100 ng/mL) were quantified on a BD Fortessa X-20.

Cryopreserved PHHs were purchased from Bio-reclamationIVT (Frankfurt, Germany) or Lonza (Melbourne, Australia) and were cultured in supplied media according to the manufacturer's specifications. PHHs were seeded in quadruplicate in 96-well plates at a density of 7.5×10^4 cells/well and rested for 6 hours. In some experiments, cells were pretreated for 1 hour with 60 μ M necrostatin-1 (Enzo Life Sciences) and 40 μ M QVD-OPh (Sigma-Aldrich). For viability assays, PHHs were treated for 24 hours with 500 ng/mL recombinant human TNF (Miltenyi Biotec, Gladbach, Germany) and 100 μ M SMAC mimetic (Birinapant, Teralogic Pharmaceuticals). Cell viability was determined using the Cell Titre Glo 2.0 assay (Promega) according to the manufacturer's instructions. For PHHs co-cultured with various stimuli in an attempt to induce RIPK3 expression, cells were plated as previously described and were treated for 16 hours with one of the following: 100 ng/mL LPS (from Salmonella; Sigma-Aldrich), 10 μ M CpG (ODN1826; Invivogen, San Diego, CA), 50 μ g/mL Poly(I:C) HMW (Invivogen), 200 ng/mL human IFN γ (Biolegend), 200 ng/mL IFN β (Peprotech, Rocky Hill, NJ), 500 ng/mL recombinant human TNF (Miltenyi Biotec), LCMV Docile at a multiplicity of infection of 1, 40 μ M QVD-OPh (Sigma-Aldrich), 80 mM ethanol (EtOH; Sigma-Aldrich), 25 μ M MG132 (Sigma-Aldrich), 50 ng/mL phorbol 12-myristate 13-acetate (PMA; Sigma-Aldrich).

Flow Cytometry

Liver tissue was passed through a 100- μ m cell strainer to generate a single-cell suspension before centrifugation at 300g for 10 minutes at 4°C. The cell pellet was resuspended in 37.5% Percoll (GE Healthcare) in PBS before centrifugation at 670g for 20 minutes at 4°C without brake. The pellet contained the lymphocyte population, which was resuspended and washed in ice-cold PBS supplemented with 2% FCS (PBS/FCS) (Gibco; ThermoFisher Scientific). Alternatively, spleen tissue was passed through a 40- μ m cell strainer to generate a single-cell suspension. Red blood cell lysis was performed using ACK buffer (150 mM NH₄Cl, 10 mM KHCO₃, and 0.1 mM EDTA). Splenocytes were washed with PBS/FCS and 2 rounds of centrifugation at 500g for 5 minutes at 4°C; 1×10^6 cells were taken for antibody staining and downstream analysis. Specific monoclonal antibodies were purchased from eBioscience (ThermoFisher

Scientific) or BD Biosciences: CD4 APC-Cy7 (RM4-5), CD8 BV510 (53-6.7), CD11b BV510 (M170), CD11c PE/Cy7 (HL3), CD19 PerCP-Cy5.5 (ID3), CD69 BV421 (H1.2F3), CD279 PE (PD1; J43), Gr1 Alexa700 (Ly6G/Ly6C; RB6-8C5), MHC-II FITC (I-A/I-E; 2G9), and CD16/32 (2.4G2). H-2D^b restricted LCMV tetramers were purchased from Baylor College of Medicine (Houston, TX) and were conjugated to APC: GP33 (KAVYNFATM) or NP396 (FQPQNGQFI). Cells were stained with tetramer for 1 hour at 4°C. All flow cytometry data were collected on a Fortessa X20 (BD Biosciences) and analyzed using FlowJo software (version 10; FlowJo LLC, Ashland, OR).

Quantitation of Pathogens

Spleen or liver tissue was removed from LCMV-infected mice for quantification. Organs were homogenized using a Qiagen (Hilden, Germany) tissueLyser and viral titers were determined by focus forming assay, using MC57 fibroblast cells, as previously described.⁵ HBV DNA was extracted from the serum using Invisorb virus DNA HTS 96 kit (Stratec Biomedical Systems, Birkenfeld, Germany) and quantification performed by real-time polymerase chain reaction (PCR) as previously described.⁶ Forty-four hours post infection, livers were dissected from CO₂ euthanized mice, suspensions generated with cell strainers, RNA purified using TRI Reagent (Sigma) and cDNA prepared with SensiFast cDNA synthesis kits (Bioline, London, UK). Quantitative reverse-transcriptase PCR was performed using a LightCycler 480 (Roche) to measure crossing points for the *P berghei* 18S ribosomal RNA subunit and mouse hypoxanthine guanine phosphoribosyl transferase (*hprt*) housekeeping gene as described previously (primers in Table 1).⁷ Parasitemia was monitored by daily examination of Giemsa-stained thin blood smears. Animals were observed daily for signs of disease, and those that developed hyperparasitemia (>15%), anemia, or neurological symptoms were CO₂ euthanized.

Isolation, Expansion, and Differentiation of Human Liver Organoids

Human liver tissues were obtained from Austin Hospital (Melbourne, Australia) with human ethics through the Austin Health Human Research Ethics Committee (HREC) (HREC/14/Austin/388). As described elsewhere,⁸ the tissues were dissected, and single cells were collected, seeded in Cultrex BME2 matrix (R&D, #RDS353301002) and expanded in expansion medium that is composed of basal medium (Advanced DMEM/F-12 (Life Technologies, Carlsbad, CA, #12634) supplemented with 1% (vol/vol) Pen/Strep, 1% (vol/vol) GlutaMAX (Life Technologies, #35050), and HEPES 10 mM (Life Technologies, #15630)) supplemented with 1:50 B27 (Life Technologies, #12587), 1:100 N2 (Life Technologies, #17502), 1 mM N-acetylcysteine (Sigma-Aldrich, #A0737-5MG), 10% (vol/vol) Rsp01 conditioned medium, 10 mM nicotinamide (Sigma-Aldrich, #N0636), 10 nM recombinant human gastrin I (Sigma-Aldrich, #G9145), 50 ng/mL recombinant human epidermal growth factor (EGF) (Peprotech, #AF-100-15), 100 ng/mL

recombinant human FGF10 (Peprotech, #100-26), 50 ng/mL recombinant human HGF (Peprotech, #100-39), and 10 μM Forskolin (Tocris Bioscience, Bristol, UK, #2939) and 5 μM A83-01 (Tocris Bioscience, #2939).

Human liver organoids were differentiated by seeding and culture in expansion medium supplemented with BMP7 (25 ng/mL) (Peprotech, #120-03P) for 5 days, and then switched to full differentiation medium, which is basal medium supplemented with 1:50 B27 (Life Technologies, #12587), 1:100 N2 (Life Technologies, #17502), 1 mM N-acetylcysteine (Sigma-Aldrich, #A0737-5MG), 10 nM recombinant human gastrin I (Sigma-Aldrich, #G9145), 50 ng/mL recombinant human EGF (Peprotech, #AF-100-15), 25 ng/mL recombinant human HGF (Peprotech, #100-39), 0.5 μM A83-01 (Tocris Bioscience, #2939), 10 mM DAPT (Sigma-Aldrich, #D5942), 3 mM dexamethasone (Sigma-Aldrich, #D4902), 25 ng/mL BMP7 (Peprotech, #120-03P), and 100 ng/mL recombinant human FGF19 (R&D, #969-FG-025).

Liver Organoid Viability Assay

Human liver organoids were seeded in BME2 matrix in 96-well plates for the differentiation process. After 7 days in full differentiation medium, human liver organoids were cultured in media for 48 hours supplemented with the experimental compounds. Cells were treated with assorted combinations of 40 μM QVD-OPh (Sigma-Aldrich) and 60 μM necrostatin 1 (Enzo Life Sciences) 1 hour before addition of 100 ng/mL recombinant TNF (Biolegend) and 10 μM SMAC mimetic (Birinapant; Tetralogic Pharmaceuticals).

To quantify for relative cell viability, the conditioned media were removed, and the human liver organoids were incubated in PBS for 15 minutes. Then, 100 mL of 5 mg/mL MTT (3,(4,5-dimethylthiazol-2-yl)2,5-diphenyl-tetrazolium bromide, Sigma-Aldrich #M2128) diluted in PBS was added into each well and the plate was incubated for 4 hours at 37°C and 5% CO₂. The supernatant was then discarded and 200 mL of lysis buffer made up of 50% N,N-dimethylformamide, 20% (wt/vol) SDS, 2.5% of 80% acetic acid, and 2.5% 1 M HCl was added. After incubating overnight at 37°C, 100 mL of supernatant was transferred to a clean flat-bottom 96-well plate and optical densities at 570 nm were determined using a BMG Lumistar plate reader.^{9,10}

Methylation Sequencing

Methylation sequencing was performed as outlined in the following using the following human cell lines and primary cell sources: HT29, human colon adenocarcinoma immortalized cell line; Huh7, human hepatocellular carcinoma immortalized cell line; HepG2, human hepatocellular carcinoma immortalized cell line; primary human PBMC; Primary human hepatocytes (PHH); HuLiver mice liver hepatocytes; human derived liver organoids.

The following mouse cell lines and primary cell sources were used: primary mouse splenocytes (C57BL/6); Hepa1-6, mouse hepatoma immortalized cell line (C57BL/6); PMH, primary mouse hepatocyte (C57BL/6); RAW, mouse macrophage immortalized cell line (BALB/c).

Bisulfite conversion. An amount of 500 ng genomic DNA was bisulfite-converted using the QIAgen Epitect Fast kit according to the low-concentration protocol. Cleanup was performed without carrier RNA, and converted DNA was eluted in 15 mL EB.

Nanopore amplicon bisulfite sequencing. A 734-bp amplicon covering 45 CpG sites in the human Ripk3 CpG island and TSS was amplified with “Nanopore CGI-1-fw+rv” primers and Kapa HiFi Uracil+ from 1 μ L converted DNA with the following PCR conditions: 98°C 2', 32 \times (98°C 10' hepatitis B core antigen'', 57°C 10'', 72°C 1'), 72°C 5', 12°C hold. A 134-bp amplicon covering 5 CpG sites of the mouse *Ripk3* promoter was similarly amplified. PCR products were cleaned up with a 1X Ampure bead cleanup and resuspended in 10 μ L water; 10 ng of amplicon per sample were prepared and barcoded with the SQK-LSK108 and EXP-NBD103 kits following the 1-pot barcoding protocol v1 (<https://docs.google.com/document/d/1ch2bb-IdGbiu9TCwUrE7FP4xsQjwHVFUQKJx6q7-v0>). Pooled libraries were sequenced on one MinION R9.4.1 flow cell. Basecalling and demultiplexing were performed with guppy 2.3.5. Adapters were trimmed with Porechop (<https://github.com/rrwick/Porechop>), and trimmed sequences filtered with awk for the 500 to 900-bp range were mapped with minimap2¹¹ onto the amplicon reference sequence previously N-masked (CG replaced by NG) and C-to-T converted (with Bismark¹²). Counts of C and T nucleotides sequenced at CG positions were collected with the RSamtools pileup function (R package version 2.6.0).¹³

Primer sequences. SRT1_OH1: 5'- CAAGCAGAAGACG-GCATACGGAGATCCGGTCTCGGCATTCCCTGCTGAACCGCTCTTC CGATCTNNNNNNNGT GACCTATGAACTCAGGAGTC-3'

SRT2-OH2: 5'- AATGATACTGGCGACCACCGAGATCTACA-

CTCTTTCCCTACACGACGCTCT

TCGGATCTNNNNNNNNCTGAGACTTGCACATCGCAGC-3'

The sequence NNNNNNNN is where individual indexes are placed in the oligo design.

Human Nanopore CGI-1-fw TTGGGGTTAACATYGGGTT-ATTAA

Human Nanopore CGI-1-rv AAAAATAAAAACCTCTTCCC product size: 734 bp.

PCR conditions: 98°C 2', 32 \times (98°C 10'', 57°C 10'', 72°C 1'), 72°C 5', 12°C hold.

Mouse Nanopore fw: AAGAATTGAAGAAGTTGGAG-TTTGT

Mouse Nanopore rv: CACTCTAACTACAACATAAAATCA-CTCA

Product size: 134 bp.

RIPK3 Overexpression and Death Assays

Cell culture. Huh7 cells were cultured in human DMEM (ThermoFisher) media supplemented with 10% vol/vol FCS (Sigma) and puromycin (1.25 μ g/mL; StemCell Technologies, Vancouver, Canada) added for lines stably transduced with pF TRE3G PGK puro empty vector or pF TRE3G PGK puro containing the human RIPK3 construct. Routine PCR testing confirmed cell lines to be mycoplasma negative.

IncuCyte cell death assay. Huh7 cells were seeded into 48-well plates at 2.4×10^4 cells/well and left to settle for 16 to 24 hours before treatment with doxycycline (500 ng/mL) overnight to induce expression of the relevant RIPK3 construct and human interferon (IFN β , 250 ng/mL) to induce expression of endogenous MLKL. Cells were then treated with TNF (100 ng/mL), the Smac-mimetic compound A (500 nM) and the pan-caspase inhibitor IDN-6556 (5 μ M) to induce necroptosis in FluoroBrite DMEM (ThermoFisher Scientific) media supplemented with 1% FCS (Sigma), 1 mM Na pyruvate (ThermoFisher Scientific), 1 mM L-GlutaMAX, and 0.25 nM SYTOX Green (ThermoFisher Scientific), as previously described.¹⁴⁻¹⁶ Cells were imaged using default bright-field and green channel settings on $\times 10$ objective in an IncuCyte SX5 System (Sartorius) with scans every hour for 20 hours. The number of SYTOX Green-positive cells per mm² over time was quantified using IncuCyte SX5 v2021B software (Sartorius).

Western blot. Huh7 cells were seeded into 24-well plates at 5.6×10^4 cells/well and induced overnight with 500 ng/mL doxycycline for RIPK3 expression, and human interferon (IFN β , 250 ng/mL) to induce endogenous MLKL expression. Cells were then treated with TNF (100 ng/mL), the Smac-mimetic compound A (500 nM) and the pan-caspase inhibitor IDN-6556 (5 μ M) to induce necroptosis in DMEM media supplemented with 1% FCS. Cells were harvested 5 hours post necroptotic induction (with TSI) in 2X SDS Laemmli lysis buffer, Lysates were boiled for 5 minutes and separated and probed with antibodies as outlined previously.

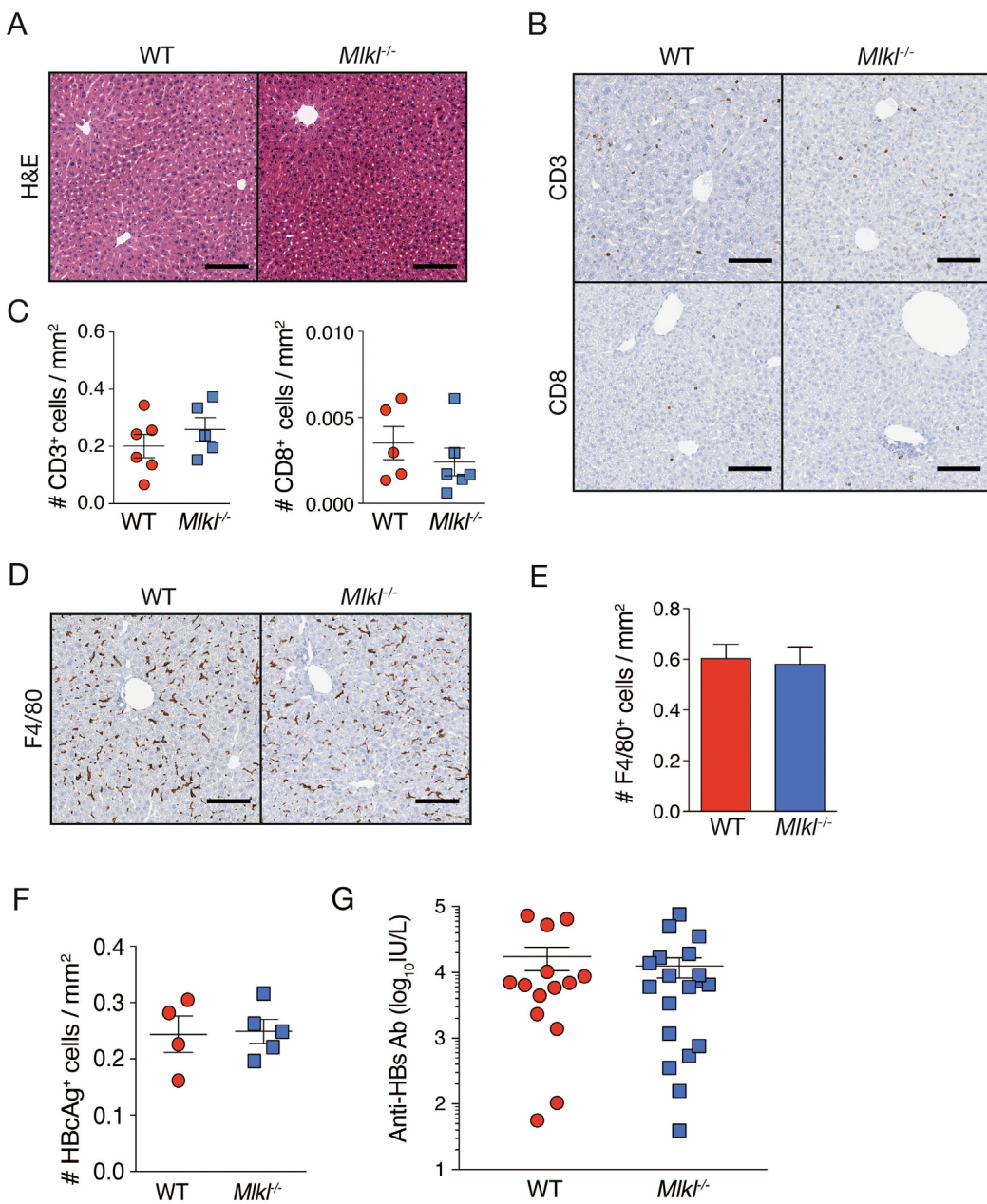
Statistical Analysis

Grouped data are represented as mean \pm SD or mean \pm SEM as indicated. Prism 6.0d software (Graph Pad Software, La Jolla, CA) was used to perform statistical tests.

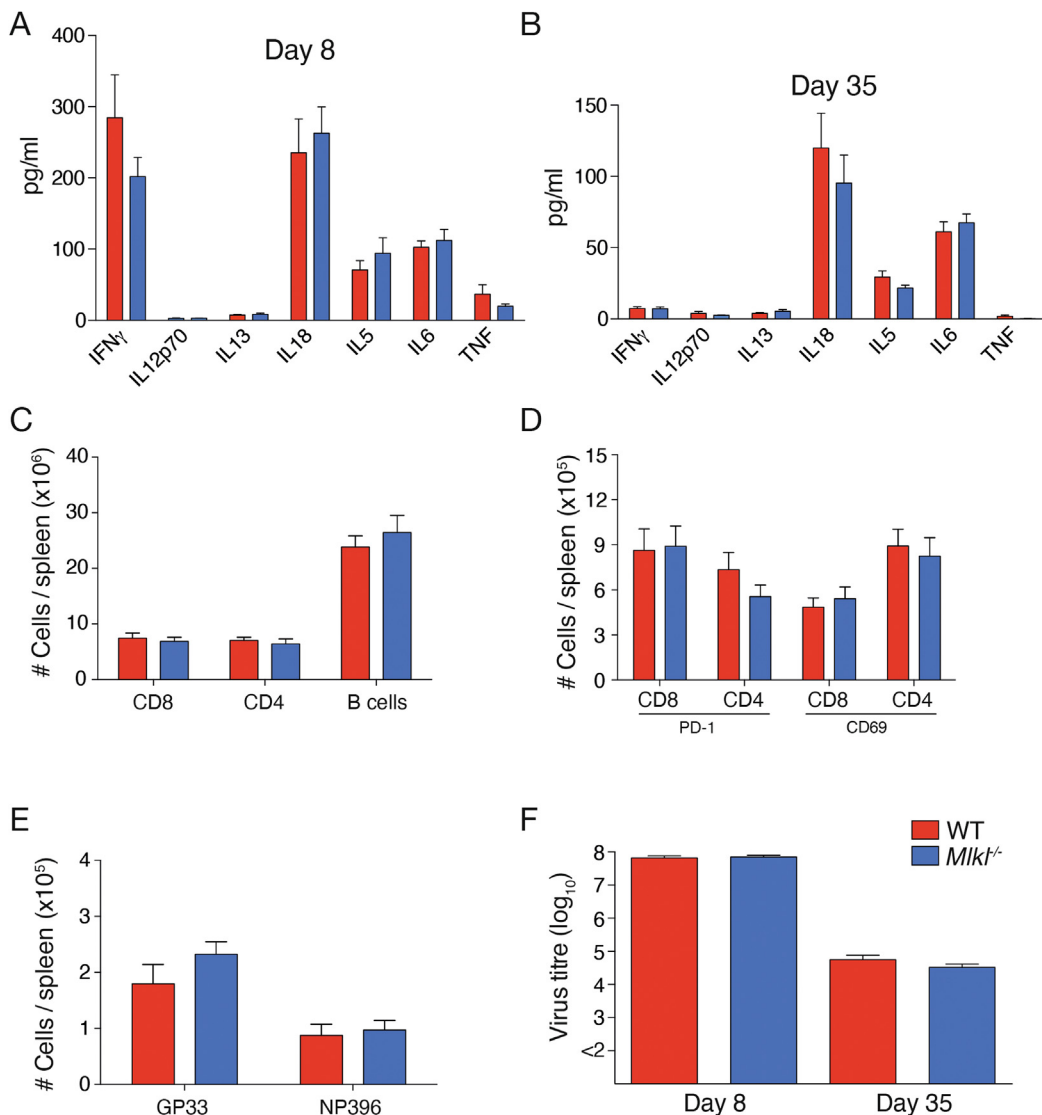
Supplementary References

1. Franke-Fayard B, Trueman H, Ramesar J, et al. A *Plasmodium berghei* reference line that constitutively expresses GFP at a high level throughout the complete life cycle. Mol Biochem Parasit 2004;137:23-33.
2. Juluri R, Vuppalanchi R, Olson J, et al. Generalizability of the nonalcoholic steatohepatitis clinical research network histologic scoring system for nonalcoholic fatty liver disease. J Clin Gastroenterol 2011;45:55-58.
3. Karunakaran D, Richards L, Geoffrion M, et al. Therapeutic inhibition of miR-33 promotes fatty acid oxidation but does not ameliorate metabolic dysfunction in diet-induced obesity. Arterioscler Thromb Vasc Biol 2015; 35:2536-2543.
4. Schindelin J, Arganda-Carreras I, Frise E, et al. Fiji: an open-source platform for biological-image analysis. Nat Methods 2012;9:676-682.
5. Battegay M, Cooper S, Althage A, et al. Quantification of lymphocytic choriomeningitis virus with an

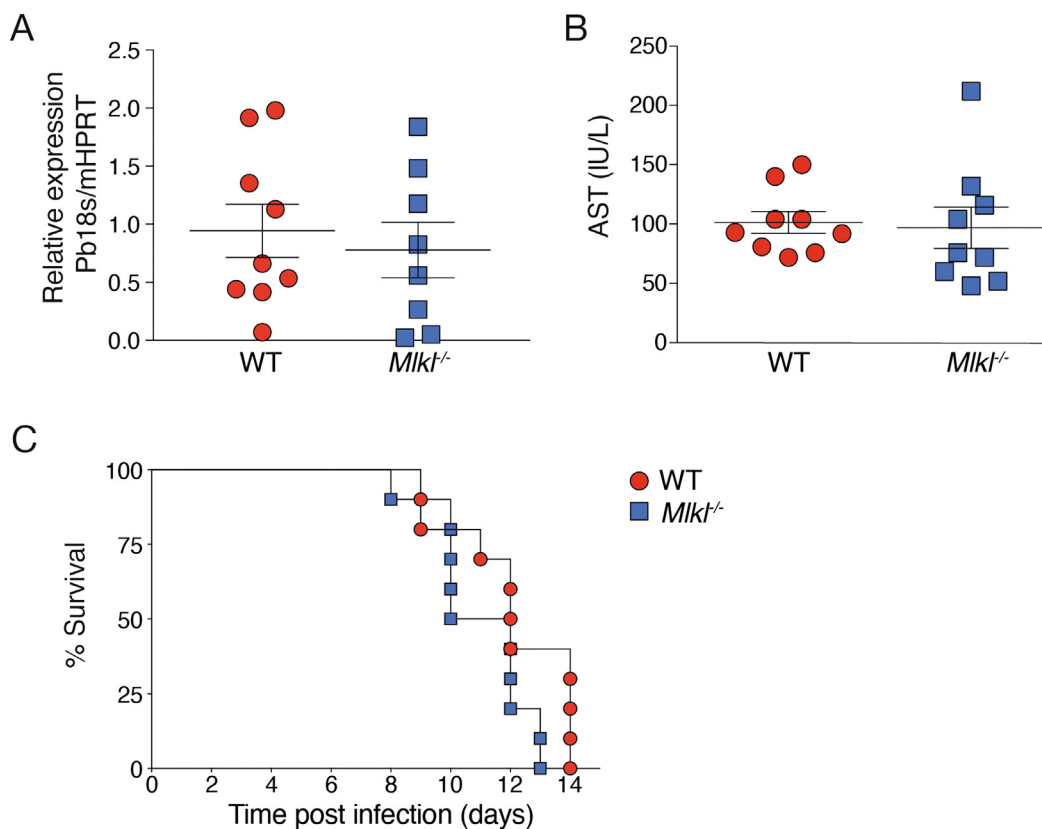
- immunological focus assay in 24- or 96-well plates. *J Virol Methods* 1991;33:191–198.
6. Ebert G, Preston S, Allison C, et al. Cellular inhibitor of apoptosis proteins prevent clearance of hepatitis B virus. *Proc Natl Acad Sci U S A* 2015;112:5797–5802.
 7. Armistead JS, Jennison C, O'Neill MT, et al. *Plasmodium falciparum* subtilisin-like ookinete protein SOPT plays an important and conserved role during ookinete infection of the *Anopheles stephensi* midgut. *Mol Microbiol* 2018; 109:458–473.
 8. Broutier L, Andersson-Rolf A, Hindley CJ, et al. Culture and establishment of self-renewing human and mouse adult liver and pancreas 3D organoids and their genetic manipulation. *Nat Protoc* 2016;11:1724–1743.
 9. Hansen MB, Nielsen SE, Berg K. Re-examination and further development of a precise and rapid dye method for measuring cell growth/cell kill. *J Immunol Methods* 1989;119:203–210.
 10. Flanagan DJ, Phesse TJ, Barker N, et al. Frizzled functions as a Wnt receptor in intestinal epithelial Lgr5+ stem cells. *Stem Cell Rep* 2015;4:759–767.
 11. Li H. Minimap2: pairwise alignment for nucleotide sequences. *Bioinformatics* 2018;34:3094–3100.
 12. Krueger F, Andrews SR. Bismark: a flexible aligner and methylation caller for Bisulfite-Seq applications. *Bioinformatics* 2011;27:1571–1572.
 13. Morgan M, Pagès H, Obenchain V, et al. Binary alignment (BAM), FASTA, variant call (BCF), and tabix file import (Release 3.12). Bioconductor 2020. Available at: <https://bioconductor.org/packages/release/bioc/html/Rsamtools.html>. Accessed October 30, 2020.
 14. Garnish SE, Meng Y, Koide A, et al. Conformational interconversion of MLKL and disengagement from RIPK3 precede cell death by necroptosis. *Nat Commun* 2021;12:2211.
 15. Samson AL, Zhang Y, Geoghegan ND, et al. MLKL trafficking and accumulation at the plasma membrane control the kinetics and threshold for necroptosis. *Nat Commun* 2020;11:3151.
 16. Meng Y, Davies KA, Fitzgibbon C, et al. Human RIPK3 maintains MLKL in an inactive conformation prior to cell death by necroptosis. *Nat Commun* 2021;12:6783.



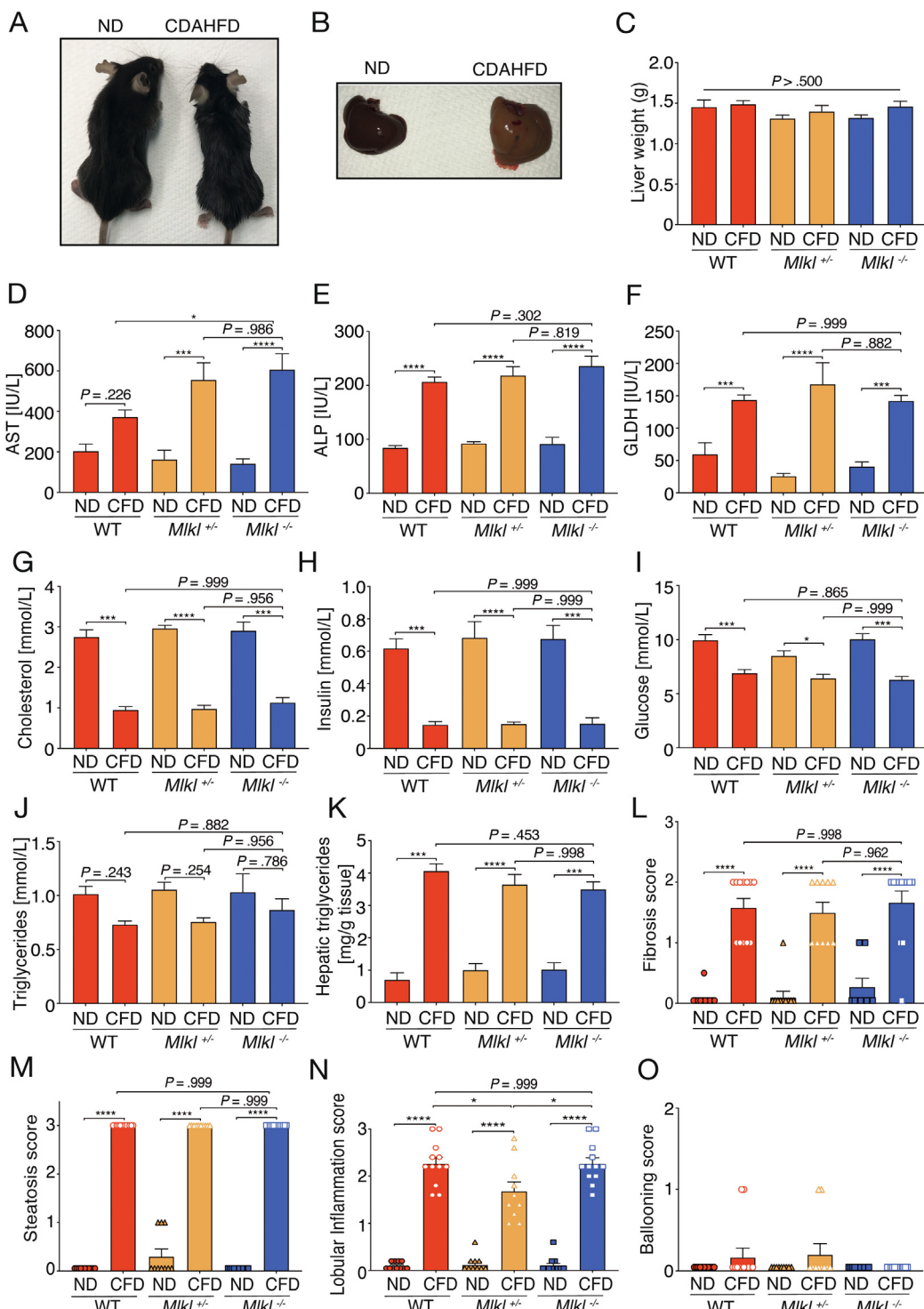
Supplementary Figure 1. (related to Figure 1). MLKL deficiency does not lead to liver abnormalities under steady state conditions or impact immunity to HBV infection. (A) Liver sections from naïve mice stained with H&E. (B) T cells with CD3 (top) or CD8 (bottom) staining by immunohistochemistry (IHC). (C) Quantitation of the cell types stained for in (B). (D) Liver sections from naïve mice stained with F4/80 by IHC to indicate Kupffer cells. (E) Graph indicates the number of F4/80⁺ Kupffer cells in the livers of naïve mice (n = 5 to 6 mice per group). (F) Quantification of hepatitis B core antigen (HBcAg) staining from liver sections of mice 14 days post induction of HBV infection. (G) Hepatitis B virus surface antigen (HBsAb) seroconversion following clearance of HBV. Symbols represent individual mice. Images are representative of at least 6 mice per group. Scale bar in (A), (B), and (D): 125 μ m. Data shown are representative of at least 2 independent experiments. Graphs show mean and SEM. HBcAG, hepatitis B core antigen.



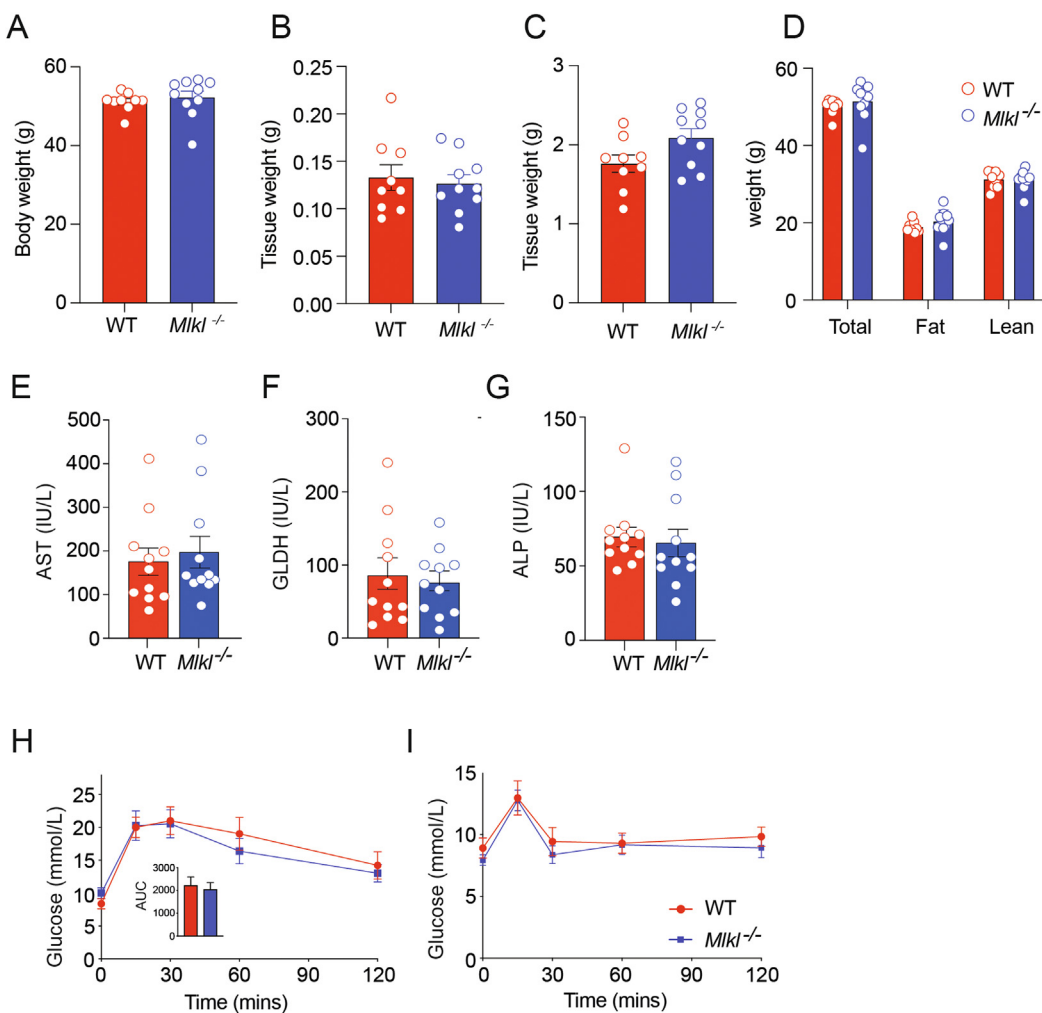
Supplementary Figure 2. (related to Figure 2). MLKL deficiency does not alter immunity to LCMV in the spleen. (A and B) Serum cytokine levels in LCMV Docile infected mice (A) 8 days and (B) 35 days post infection (n = 8 mice per group). (C) Flow cytometric determination and enumeration of the absolute numbers of the indicated immune cells harvested from spleens of LCMV Docile infected mice (n = 8 mice per group). (D) Numbers of splenic, antigen activated T cells that express PD-1 or CD69 (n = 8 mice per group). (E) Flow cytometric determination of the absolute number of LCMV-specific CD8 $^{+}$ T cells, recognizing the indicated viral epitopes, harvested from the spleens of LCMV-infected mice (n = 8 mice per group). (F) Virus titers in the spleens of infected mice at days 8 and 35 post infection (n = 8 mice per group). All data in this figure were generated from mice taken 8 days post infection with LCMV Docile unless stated otherwise. Data shown are the combined data from 2 independent experiments. Graphs indicate the mean and SEM.



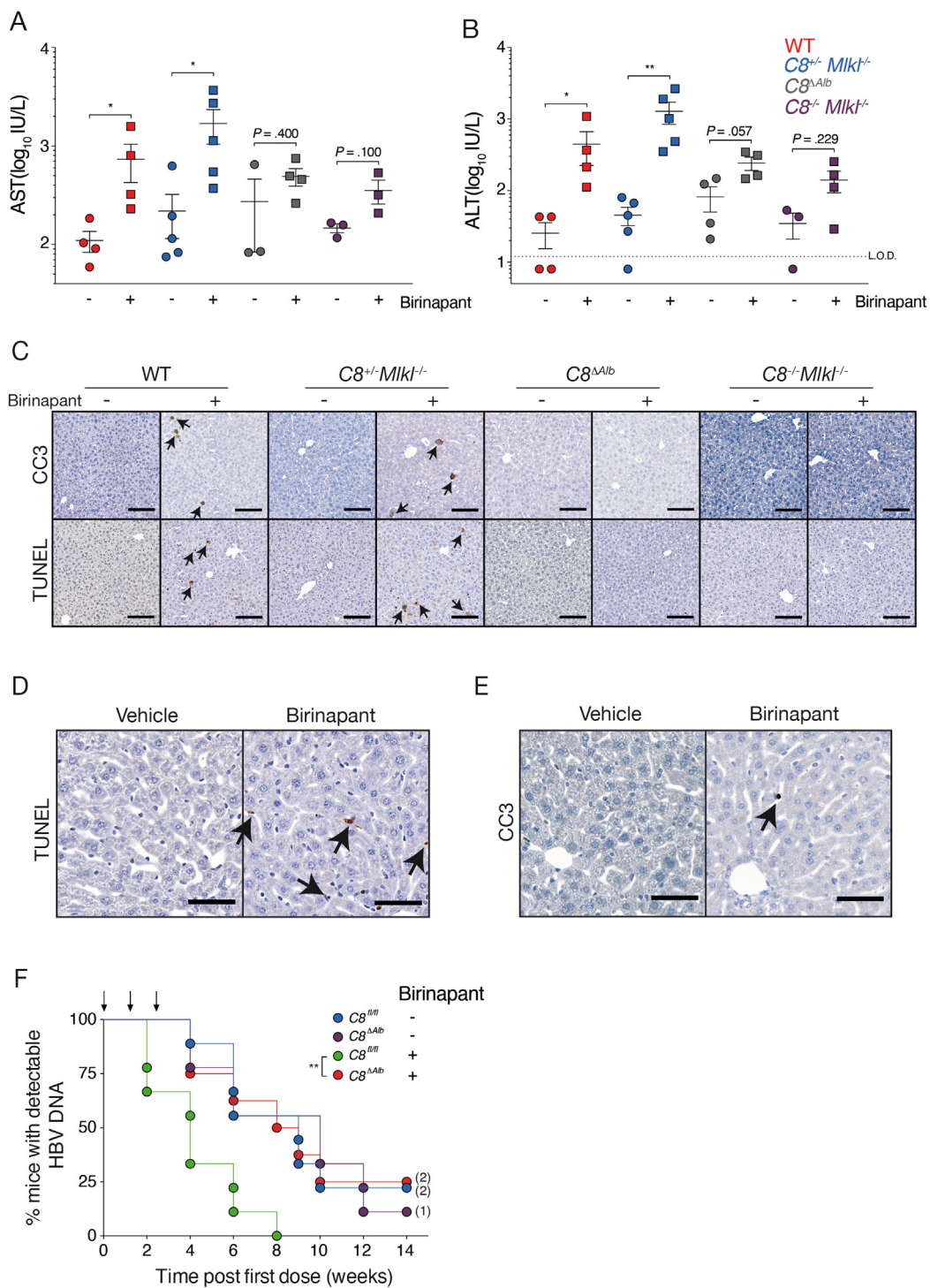
Supplementary Figure 3. Necroptosis does not affect liver-stage infection of malaria parasites in mice. (A) Quantitative reverse-transcriptase polymerase chain reaction (qRT-PCR) of *P. berghei* 18S relative to mouse HPRT in the livers of mice 44 hours post infection with sporozoites. (B) Serum levels of AST from mice 44 hours post infection. (C) Proportion of animals and time when mice either developed illness (cerebral malaria) or they achieved a blood parasitemia >15% (euthanasia endpoint). Graphs show combined data from 2 independent experiments. Mean and SEM are indicated.



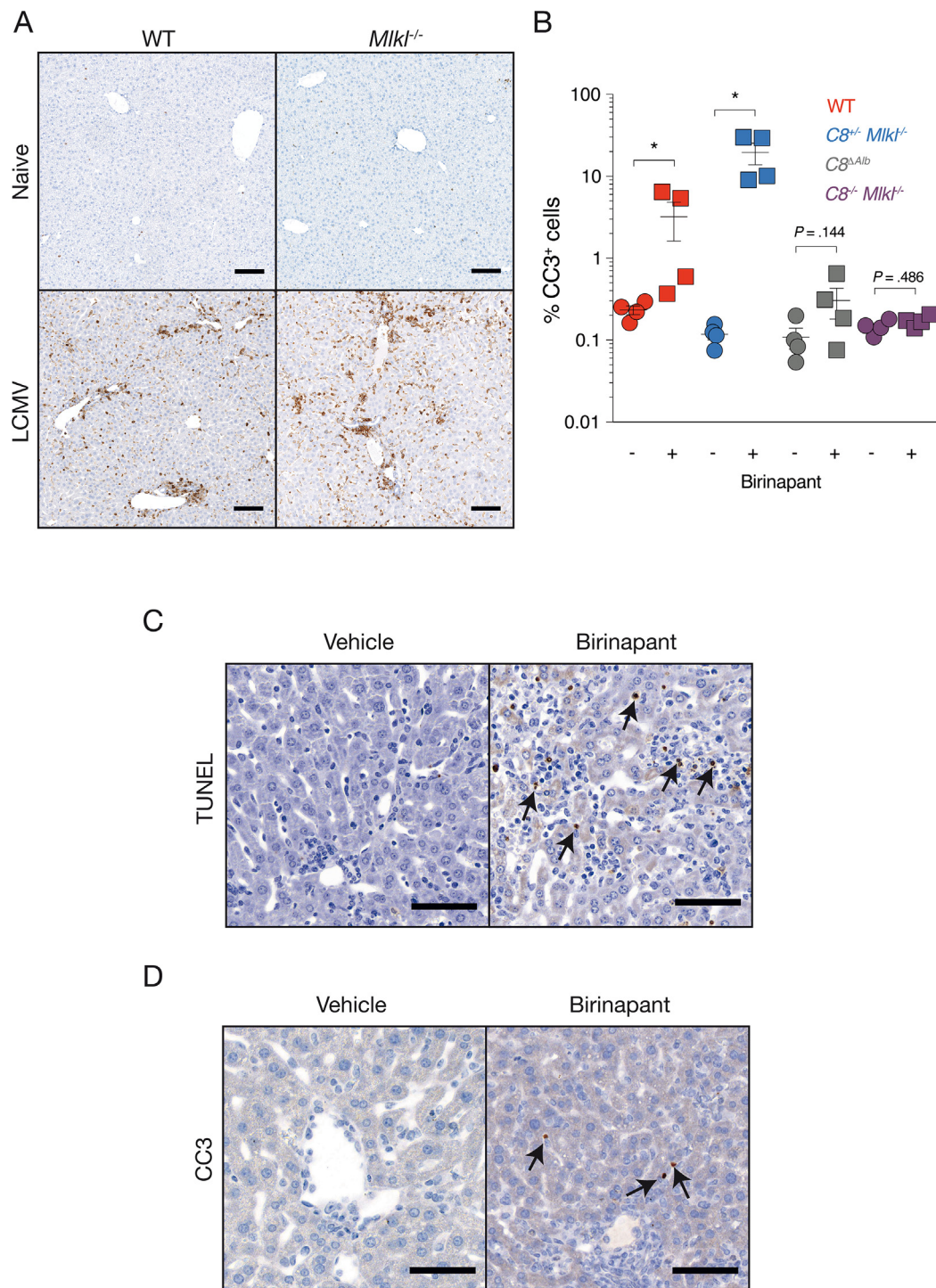
Supplementary Figure 4. (related to Figure 3). MLKL deficiency does not affect development and outcome of CDAHFD-induced NASH. Representative images of (A) WT mice and (B) their livers that were either fed a normal diet (ND) or a CDAHFD (short CFD) for 8 weeks. (C) Total liver weight after 8 weeks on the indicated diet. (D–J) Levels of (D) AST, (E) ALP, (F) glutamate dehydrogenase (GLDH), (G) cholesterol, (H) insulin, (I) glucose and (J) triglycerides in the plasma of animals after 8 weeks on the indicated diet. All graphs are $n = 10\text{--}12$ except (F), which is $n = 7\text{--}11$. (K) Concentration of triglycerides in the liver of mice after 8 weeks on the indicated diet ($n = 10\text{--}12$). (L) Fibrosis score, (M) steatosis score, (N) lobular inflammation, and (O) ballooning score of liver sections scored by a pathologist. Error bars represent SEM. * $P < .05$, ** $P < .005$, *** $P < .001$, **** $P < .0001$ (1-way analysis of variance followed by a Tukey's multiple comparisons test).



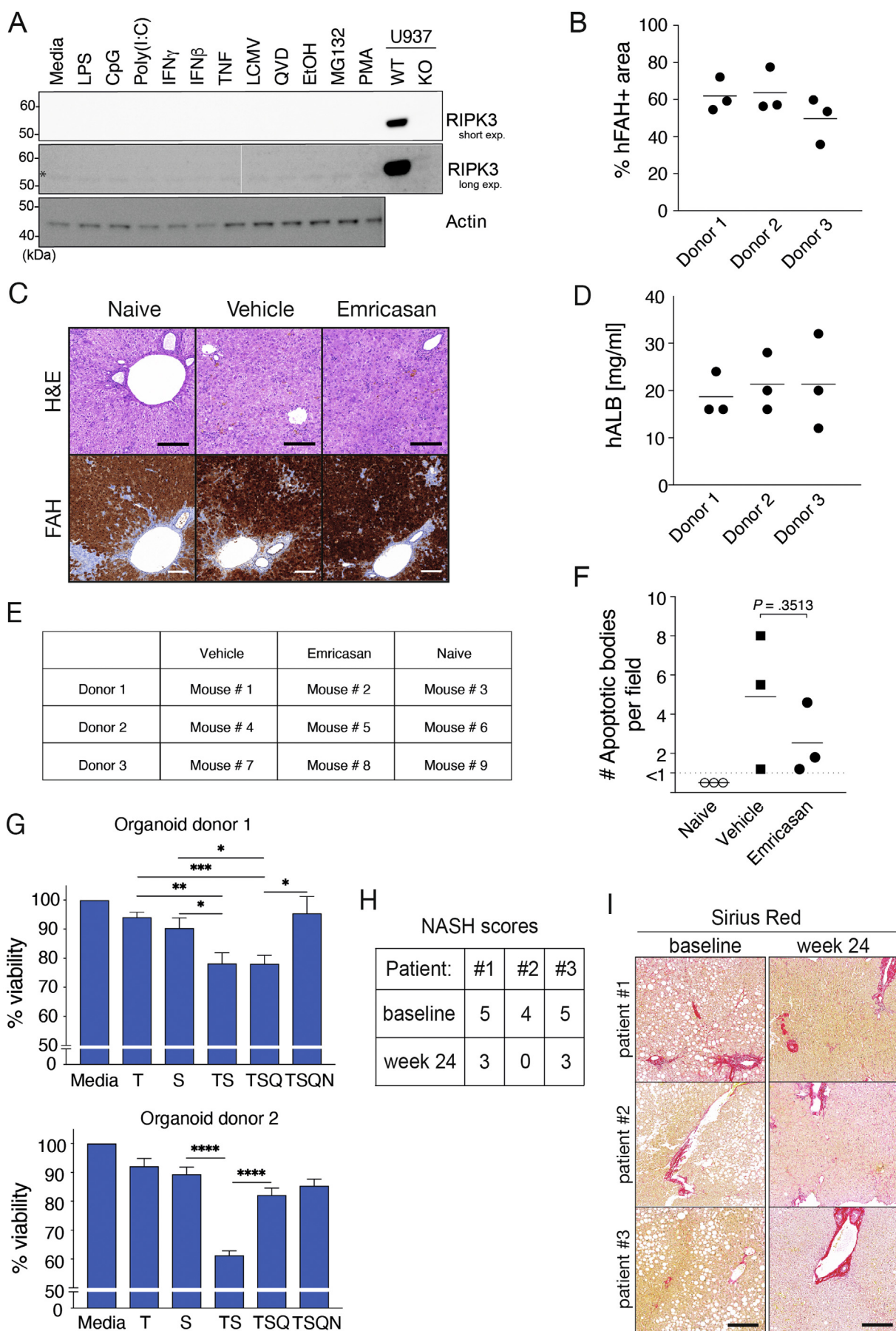
Supplementary Figure 5. (related to Figure 3). MLKL deficiency does not affect development and outcome of HFD-induced NASH. WT or MLKL-deficient mice were fed on a 60% kcal HFD, containing choline. Body weight was measured weekly and organ weights were measured at the end of the experiment. (A) Total body weight, (B) spleen weight, (C) adipose tissue (perigonadal) weight, and (D) fat and lean mass are shown. Levels of plasma (E) AST, (F) glutamate dehydrogenase (GLDH), and (G) ALP measured at 24 weeks. (H) Glucose tolerance test (GTT) and (I) Insulin tolerance tests (ITT) performed on mice receiving an HFD ($n = 9\text{--}10$ mice per group). Each symbol represents 1 mouse. Error bars represent SEM.



Supplementary Figure 6. Hepatocyte-specific loss of caspase-8 prevents SMAC-mimetic induced clearance of HBV in mouse model. WT or MLKL-deficient mice were infected with HBV and 7 days later treated with or without SMAC mimetic. Serum (A) AST and (B) ALT were quantified 16 hours after treatment with vehicle (-) or birinapant (+). (C) Liver sections from mice described in (A) and (B) were analyzed by immunohistochemistry (CC3; top or TUNEL; bottom). Scale bar: 125 μ m. (D) Higher-magnification images of sections of liver tissue from $C8^{\Delta Alb}$ animals from (C), where brown staining indicates (D) TUNEL+ or (E) CC3+ nonhepatocytes (arrows). Scale bar: 62.5 μ m. (F) Proportion of animals and time when mice of the indicated genotypes were treated with vehicle (-) or birinapant (+) first achieved an undetectable serum HBV DNA level. Mice were treated 3 times as indicated (arrows), starting 1 week post infection. Numbers next to dots in the time-to-event analyses represent the number of mice that have not cleared HBV. Images in (C-E) are representative of at least 10 histological specimens. Data are representative of 2 independent experiments (A and B) or the combined data of 2 independent experiments (F). LOD, limit of detection; * $P < .05$. ** $P < .001$ (A and B, u-test; F, log-rank Mantel-Cox test).



Supplementary Figure 7. (related to Figure 4). Necroptosis is restricted in mouse hepatocytes *in vivo* even under highly inflammatory conditions. (A) Representative histological images of liver sections stained with antibodies recognizing CD3, from mice of the indicated genotype that were left uninfected (naïve; top) or infected with LCMV Docile (LCMV, day 8 post infection; bottom). Scale bar: 125 μ m. (B) Quantification of the proportion of CC3⁺ cells in the liver from experiment in Figure 5B–E. (C and D) Representative histologic images of liver sections from LCMV-infected C8^{ΔAlb} mice (day 8), taken 16 hours after treatment with birinapant or vehicle and stained with antibodies (C) recognizing total cell death (TUNEL) or (D) apoptosis (CC3). Arrows indicate dead/dying cells that do not appear to be hepatocytes. Scale bar: 62.5 μ m. Images are representative of at least 8 analyzed histologic specimens.



Supplementary Table 1. Oligonucleotides Used to Determine *P. berghei* Liver Parasite Load

Primer name	Sequence
Pb18s <i>fwd</i>	GGAGATTGGTTTGACGTTATGTG
Pb18s <i>rev</i>	AAGCATTAAATAAAGCGAATACATCCTTAC
mHPRT <i>fwd</i>	CATTATGCCGAGGATTGGA
mHPRT <i>rev</i>	AATCCAGCAGGTCAAGCAAAG

◀ **Supplementary Figure 8.** (related to Figure 5). Primary human hepatocytes fail to undergo necroptosis in vitro and in vivo. (A) Western blot analysis of lysates from PHHs, following culture with the indicated compounds for 16 hours. A short exposure (short exp.) and long exposure (long exp.) blot are shown for RIPK3. * denotes a nonspecific band. (B) Quantitation of the proportion of liver cells from HuLiver mice that were FAH⁺ (human). This was determined from the histological slides represented in (C; bottom). (C) Representative liver sections taken from HuLiver mice; experimental conditions are indicated. Sections were either stained with H&E (top) or antibodies that recognize FAH (identifying human hepatocytes; second panel). Scale bar: 125 μm. (D) Serum human albumin (hALB) from HuLiver mice determined at euthanization. Graph represented by donor along the x-axis. (E) Table illustrating the origin of, and treatment of, human cells in the HuLiver mouse experiment. (F) Number of apoptotic bodies observed by a pathologist in H&E sections from HuLiver mice. (G) Primary human liver organoid cells from donors 1 and 2 (from Figure 6F) were co-cultured with the indicated compounds and viability was measured. (H) NASH score of 3 human patients at baseline and after 24 weeks of diet change. (I) Sirius Red stain of representative liver sections from 3 human patients with NASH at baseline or 24 weeks after dietary intervention. Scale bars: 100 μm. Data are representative of 2 (A) or 1 (B–E) independent experiments. Enumeration of apoptotic bodies in (E) was performed blinded by an expert pathologist. T, TNF; S, SMAC mimetic; Q, QVD-OPh; N, necrostatin-1. *P < .05, **P < .005, ***P < .001, ****P < .0001 (unpaired t-test).